Green trend of light extinction in canopy: new construction on image mining

Abbas Haghshenas[1], Yahya Emam[2*]

[1]PhD student of Agronomy, Department of Crop Production and Plant Breeding, Shiraz University, Shiraz, Iran.

[2]Professor, Department of Crop Production and Plant Breeding, Shiraz University, Shiraz, Iran.

[*]Corresponding author. Email: yaemam@shirazu.ac.ir

Abstract

Light extinction is the most fundamental aspect of green canopies. The exponential form of light gradient is extensively evaluated or utilized by conventional approaches mainly in contribution to the vital concept of leaf area index (LAI), which reasonably characterizes canopies based on their theoretical capability for light attenuation i.e. having greater leaf surfaces. We analyzed the image archive of heterogeneous wheat canopies (cultivar mixtures), captured from experimental plots of a two-year field study conducted at College of Agriculture, Shiraz University, Iran, to evaluate the option of using commercial digital cameras for comparing the canopies based on their relative optics, and also providing new representation of light extinction within the canopy. Here, two novel distinct techniques including different imaging and calculation methods were employed. In the first one, or Green-based Segmentation Model (GSM), pixels of vegetation parts were categorized into "*n*" light-to-darkness groups based on their similar Green values (RGB color system). Then, mean red, mean green, and mean blue values of each group were calculated and their separate trends were plotted against the mentioned green light-to-dark steps. In the second method, a kind of *in-situ* spectroscopy of sun-exposed leaves (DLBE, Double-shot Light Balance Equations) was evaluated under the isotropic scattering assumption, with the aim of estimating the absorbed portion of light by sun-exposed leaves, using reflected and transmitted portions. Facing the sun, and then with the sun behind the camera, two images

were taken from each plot; in which "*Transmission*" and "*Reflection*" ROIs (ranges of interest) were extracted, respectively. Finally, normalized color values were calculated using mean RGBs of either type of ROI. Results of GSM showed that the green-scaled gradient of reflected red and blue lights had robust exponential trends which could be readily utilized for identifying canopies in the form of one or two image-derived equation(s). Various "canopy-light" interactions are categorized in detail by segmenting the most precise version of GSM curves (255-tuple GSM) based on relative slopes, and consequently, reconciling the resulted ranges with images. Moreover, evaluating curve characteristics (in 255-tuple GSM) revealed new aspects of light status within canopy e.g. (a) main portions of red and blue light extinction occur in different (leaf) surface angles; (b) completely-shaded parts of various canopies behaved significantly different in light interactions; and, (c) environmental stresses changed the curvature of red and blue curves. The results of orthogonal equations of DLBE proposed that wheat mixture treatments were significantly different only in absorption of green and blue light by sun-exposed leaves. Besides, an unexpected observation of grain yield simulation by the red color level of the canopy background (soil) is reported. We believe that the image-based computational frameworks and definitions proposed, which are straightforward, simple, and independent of LAI, may provide a novel representation of light extinction and also open new windows to the monitoring of light gradient in canopies.

Keywords

Canopy spectroscopy, cultivar mixture, digital camera, grain yield, GSM model, wheat.

1. Introduction

Vegetation canopies are identified based on how they interact with light. In plant communities of natural environments, a theoretical simple arrangement of a single unshaded layer of (green) leaves would provide potentially the basic light conditions for photosynthesis; though, such conceptually integrated light-exposed surface is actually distributed in a sophisticated manner over a three dimensional structure, which inevitably casts a shadow on itself. Moreover, the shading pattern of canopies shows large tempo-spatial variations (e.g. due to time, season, plant growth stage, altering growth behaviors, biotic and abiotic stresses, etc.) which makes it even more difficult to approach coincidentally a comprehensive, efficient, and easily applicable characterizing framework.

Researches with the aim of evaluating the light-to-darkness gradient (light extinction trend) in vegetation canopies, have utilized a relatively broad spectrum of physical bases, mathematical models, and practically, novel photometric instruments (Welles and Cohen, 1996; Gower *et al.,* 1999; Jonckheere I. *et al.,* 2004; Omasa *et al.,* 2006; Jacquemoud *et al.,* 2009; Zhao *et al.,* 2011; Glatthorn and Beckschäfer, 2014; Bauer *et al.,* 2016; Yao *et al*., 2016). Despite the diversity and evolution of the methodologies, the two early introduced concepts of leaf area index –LAI- (Watson, 1947) and the exponential trend of light attenuation (i.e. based upon Beer-Lambert law; Monsi and Saeki, 2005), solely or in combination, have been the cornerstones of almost every conventional analyses in this context. Accordingly, leaves (with their individual characteristics e.g. type, angle, configuration) act as the light attenuating materials, and LAI is comparable with the material concentration. Conventional measurement approaches include estimating the conceptual index of LAI either by destructive sampling or indirect methods (Weiss *et al*., 2004; Behera *et al*., 2010; Liu *et al.,* 2010; Viña *et al*., 2011), and/or modeling the light extinction trend based on recorded light intensities by *in situ* sensors *(*Jonckheere *et al.,* 2004; Munier-Jolain *et al.,* 2013; Xue *et al.,* 2015; Perot *et al.,* 2017). In these methods, estimations are based on the light intensities in "*spaces*" within the canopy (which are considered either as the model input or output); and to the best of our knowledge, there is no report on using the reflected light from canopy green "*surfaces*" (even results of remote sensing methods in plant science –also with no claim of evaluating the light gradient- are calibrated based on LAI, or data collection from the intra-canopy spaces). It is expected that potential surface-based approaches would require a completely different estimation framework compared to the current ones, mainly due to the inclusion of a complex interaction between the status of leaf surface exposure, and leaf spectral behavior. However for the same reason, if designed properly, such an approach may represent a more precise and informative description of light status within the canopy.

The high spectral overlap between electromagnetic radiation of visible light and photosynthetically active radiation (PAR, i.e. about 400-700 nm wavelengths, McCree, 1972), provides the opportunity of using digital cameras in plant sciences as both reliable and readily available sensors of remote sensing. Employing commercial digital cameras along with most often basic image processing techniques, an increasing number of studies have reported robust correlations between various image-derived indices and crop criteria including nitrogen status (Li *et al.,* 2010; Wang *et al.,* 2013; Lee and Lee, 2013), crop growth

(Sakamoto *et al.*, 2012; Lee and Lee, 2013), chlorophyll content (Hunt Jr *et al.*, 2013), leaf area (Easlon and Bloom, 2014), leaf angle (Zou *et al.*, 2014), selection criteria for breeding programs (Casadesús *et al.*, 2007), etc. However, there is no report in the literature about using digital images for evaluating the light gradient in the canopy, or even considering the pattern of variations in the reflected light (which is recorded as pixel color values).

As in many other fields of empirical sciences, sampling (for statistical analyses) is a fundamental factor in crop/plant physiological assessments; where probably the most significant power of digital cameras lies. A typical 8-megapixel color image taken from a low height above the crop canopy, for instance, may provide a huge physiological sample included (e.g. given an 80% canopy coverage) more than 6 million pixels analogous to individual real green points (probably of various sizes). In addition to spatial resolution, high color sensibilities (e.g. the ability of discriminating over 16 million – or 256^3- colors per pixel in a common 24-bit color depth) have made it possible to record an acceptable number of 256 different mono-color intensities of light reflected in either red, green, and blue bands for a single pixel (the range of 0 to 255, for complete darkness to full radiation of a single color sensed). Processing the certainly adequate data-set provided by such a unique light sampling tool, requires subsequently more efficient data mining and computational approaches in order to improve our knowledge of the canopy light extinction.

The purpose of the present study was evaluating the option of using commercial digital cameras for (i) comparing cultivar mixtures based on the optics of their heterogeneous canopies, and (ii) providing an alternative image-based definition (and associated computational frameworks) for light extinction in the canopy.

Using two different novel techniques with distinct imaging and image processing methods, we processed a relatively considerable archive of images taken over the growing season from an experimental wheat field. The two-year field experiment consisted of 90 plots in which 15 mixture treatments including every mono- and mixed cropping of 4 early to middle ripening wheat cultivars were arranged under two post-anthesis water stressed and normal conditions in 3 replicates (thus, there were 6 identical replicates until anthesis). Such treatments could simulate a spectrum of mono-species canopy complexities from conventional homogenous stands to almost extremely heterogeneous mixtures of three or four cultivars with different phenology and/or growth characteristics. Based on the study purposes and methodological requirements, here we focus on reporting the findings resulted from a certain imaging date unless mentioned otherwise (i.e. booting stage in the first season, see the Materials and

Methods section). It is also notable that: (a) a common digital camera was deliberately chosen as the only sensor or measuring tool used (except for grain yield weight in the final section); (b) argumentations are based on either RGB color values, or normalized RGBs; and we did not report any absolute values of light quantities (i.e. in the SI system).

2. Materials and Methods

2.1. Field experiment

The field experiments were conducted at the research field of Agricultural College of Shiraz University, Iran (29°73´ N latitude and 52°59´ E longitude at an altitude of 1,810 masl). In both growing seasons, the experiment consisted of 90 (2×2 meter) plots including every 15 monocultures and mixtures of four early to middle ripening wheat cultivars under two normal and post-anthesis deficit irrigation conditions in 3 replicates (so that there were 6 replicates available in the time of imaging i.e. booting phase). The experimental design was RCBD (Randomized Complete Block Design) in a lattice arrangement with 1 meter distances between the plots. The statistical analyses for image-derived criteria and grain yield in 6 replicates were carried out as CRD (Completely Randomized Design), while the factorial analysis of grain yield in 3 replicates (including the effect of irrigation) was performed based on RCBD. The early to middle ripening wheat cultivars used were Chamran (1), Sirvan (2), Pishtaz (3), and Shiraz (4), respectively. For providing mixtures, seeds of the cultivars were mixed before sowing on flat beds, with equal ratios based on their 1000-grain weights, germination percentages, and the fixed planting density of 450 plants per square meter. The planting dates in the first and second growing seasons (2014-15 and 2015-16) were November 20 and November 5, respectively. Depending on soil test, only nitrogen fertilizer (urea) was applied, 3 times i.e. in planting, early tillering, and anthesis, with a total amount of 150 kg N/ha. No chemical was used, and weeding was done by hand.

Irrigation interval was 10 days based on local practices. From the first irrigation after anthesis, deficit-irrigated plots were irrigated with water sufficient to meet 50% of evapo-transpirational demand (calculated based on Fao-56 Penman-Monteith model with local corrected coefficients; Razzaghi and Sepaskhah, 2012; Shahrokhnia and Sepaskhah, 2013). Late in the season, plants were harvested from the center of plots (overall row length of 3 meter, or 0.6 m^2 per plot) and grain yield was calculated using a laboratory thresher and weighing.

2.2. Imaging

In the first technique, or Green-based Segmentation Model (GSM), images were taken at booting stage (April 24, 2015) from a "*normal observer's point of view, NOPOV*" (vertical top-down view), 150 cm above the soil surface (about one meter above the top of the canopy). At this growth stage, wheat stand can provide a desirable typical canopy, i.e. a sufficiently dense canopy (most leaves are fully emerged and still thoroughly green); moreover, spikes are not emerged yet (which also might be included in analyses as green organs otherwise). We used a common commercial digital camera (Canon PowerShot SX100 *IS*) which was set to auto mode and the maximum imaging resolution of 8.0 megapixels. These images were also used for the evaluation of the last section (i.e. the relationship between relative background red color level and grain yield).

In order to take the special pairs of image for the second technique, Double-shot light balance equations (DLBE), we designed a natural lighting condition by timing. Here, we needed to have a "*transmission perspective*" which can be defined briefly as an imaging/or observing view from which, related to the sample size (e.g. an experimental plot) a considerable green surface scattering the transmitted sun light (into the forward half-space) is recognizable, so an adequate sampling of light transmitted through a single leaf-layer is possible. Therefore, on this date, imaging was carried out 2 hours after solar noon, when all of the imaging practices of the experiment (from 3 points of view i.e. normal, transmission, and reflection perspectives) were done immediately for each plot. The zenith and azimuth angles at the beginning of imaging (i.e. 15:00 pm) were 57.08° and 245.71°, respectively; and the sky was clear. The overall imaging duration was 35 minutes, whose statistical effect (variation) was expected to have been determined and excluded from the analyses by the arrangement of plots in statistical designs. For imaging from the "*front*" and "*back"* points of view (i.e. for transmission and reflection perspectives), we took images from 1 meter (horizontal) distance and the same height of 150 cm, facing the sun, and then with the sun behind the camera, respectively.

Images used in phenology and stress evaluations were selected from the second season's archive (2015-16, due to occurrence of the cold stress, and more frequent imaging practices continued until the canopy dried completely). We also took and analyzed images from a reflection perspective (backward half-space) of some kinds of canopies, as other samples (Fig. S10).

2.3. Image processing and data analyses

Image processing for the whole analyses, except for the DLBE technique, was carried out using exclusive MATLAB codes (including 3 different codes; MATLAB 2015b).

2.3.1. Green-based Segmentation Model (GSM)

Following a common segmentation of each *NOPOV* image into vegetation and background parts (segmentation type 1, ST1), pixels of vegetation parts were categorized into "*n"* light-to-darkness groups based on their similar Green values (segmentation type 2, ST2; RGB color system). Then, mean red, mean green, and mean blue values of each group were calculated and their separate trends were plotted against the mentioned green light-to-dark steps. The ST1 or the common extraction of vegetation from background was performed in RGB color system using the "*green>red*" thresholding (i.e. selecting the image pixels whose green values are greater than red, as vegetation; Wang *et al.*, 2013). This thresholding was included in the three MATLAB codes for every analysis.

For ST2 (segmentation type 2) which categorizes vegetation pixels into *n* (i.e. 3 to 255) dark-to-light equal segments, the green color was selected as the basic single band for gradient scaling. Although we had red, blue, grayscale, and other criteria as alternatives for green for dark to light scaling, green band was preferred due to obviously having the most rigorous reflection from vegetation, which is expected to provide the most robust signal and also determines the vegetation barriers more accurately and precisely, compared with red and blue. In addition, it is the direct record of reflection in a given band without any conversion or adjustment, despite other formula-based indices, e.g. the synthesized grayscale.

The 255-tuple GSM with high-resolution curves (having the maximum possible number of green steps i.e. 255) were considered for further evaluations. For interpreting the red and blue trends in 255-tuple GSM, each color curve was segmented into 5 apparent parts based on significant changes in the curve local slopes (differentiations) compared with the slope of the green line (i.e. equals one). This curve segmentation method was named segmentation type 3 (ST3), based on which consequently, vegetation in respective images was also segmented into 5 light-to-darkness parts. For this purpose, the five Green ranges (RGB system) resulting from the ST3 curve segmentation were used as the inputs for color thresholding, so that the vegetation pixels with the green values in each curve-derived range were selected as an image segment.

Mathematical analyses (for equation fitness and ST3) were carried out using Origin Pro 8 software (OriginLab, Northampton, MA). The thresholding values for ST2 in 3- to 10-tuple GSMs were calculated easily by dividing the green range of 0-255 into the equal purposed subranges. The nonlinear equations evaluated for light gradients, were the simple exponential and polynomial forms as shown below:

$$Polynomial \begin{cases} R = a_R(G^2) + b_R(G) + c_R \\ B = a_B(G^2) + b_B(G) + c_B \end{cases} \quad (1)$$

$$Exponential \begin{cases} R = a_R . e^{b_R . G} \\ B = a_B . e^{b_B . G} \end{cases} \quad (2)$$

where R, G, and B are red, green, and blue colors, and a, b, c are equation constants.

Local- and linear-slopes of the red and blue curves of 255-tuple GSMs were calculated as respective differentials ($\frac{dR}{dG}$ or $\frac{dB}{dG}$) and tangents ($\frac{\Delta R}{\Delta G}$ or $\frac{\Delta B}{\Delta G}$) in defined ranges ("R", "G", and "B" are red, green, and blue, respectively; Fig. S3). Furthermore, curve area calculations (including separate or total area under red or blue curves, and various between-curve areas) were carried out using definite integrations. For instance, total AUCs (under curve areas) for red or blue curves were estimated by:

$$AUC_R = \int_{G_1}^{G_{255}} (a_R . e^{b_R . G}) dG \quad (3)$$

$$AUC_B = \int_{G_1}^{G_{255}} (a_B . e^{b_B . G}) dG \quad (4)$$

where G is green light (RGB color system), G_1 and G_{255} are low and high limits, a_R, a_B, b_R, b_B are the exponential coefficients for red and blue lights. We should emphasize that the lower limit of such total integrals are equal to 1, because 0 implies complete darkness (non-detectable reflections), while based on the ST1 thresholding (G>R, segmentation type 1), vegetation pixels lack this value. Moreover, the total BCAs (between-curve areas) of green-red, green-blue, and red-blue were determined as:

$$BCA_{G-R} = \int_{G_1}^{G_{255}} (a_G . G + b_G) dG - \int_{G_1}^{G_{255}} (a_R . e^{b_R . G}) dG \quad (5)$$

$$BCA_{G-B} = \int_{G_1}^{G_{255}} (a_G . G + b_G) dG - \int_{G_1}^{G_{255}} (a_B . e^{b_B . G}) dG \quad (6)$$

where a_G and b_G are the coefficient and constant for linear equation of green trend; and:

$$BCA_{R-B} = \int_{G_1}^{G_{255}} (a_R . e^{b_R . G}) dG - \int_{G_1}^{G_{255}} (a_B . e^{b_B . G}) dG \quad (7)$$

The definite integrals for every distinct curve segments (ST3) were also calculated in a similar way. It is notable that here, we have estimated various AUCs or BCAs based on the equations of the fitted trend lines; however, depending on the purposes, the actual-AUCs or BCAs may also be calculated using the summations of red or blue values in the specific ranges. For instance, the $Actual\ AUC_R$ may be calculated as:

$$Actual\ AUC_R = \sum_{i=1}^{255} R_{G(i)}$$

where i shows the Green level (step), and $R_{G(i)}$ is the mean Red value in the ith Green level.

The curve characteristics of the 255-tuple GSM were defined as primary and secondary indices, depending on whether they were the result of a direct calculation of a property on the curve (e.g. an area value), or were synthesized by further calculations using the primary ones (for example, most of curve ratios provided, e.g. the ratio of linear slopes of $(3-4)/(1-2)$ segments for red color). Following estimating curve differentials and integrations by Origin Pro (as mentioned), primary and secondary curve characteristics were calculated in formulated excel sheets. Statistical analyses were carried out using IBM SPSS Statistics for Windows, Version 19.0 (Armonk, NY: IBM Corp.) and all mean comparisons were performed by Tukey's test.

2.3.2. Double-shot Light Balance Equations (DLBE)

From the physiological point of view, the light absorption by the sun-exposed leaf surfaces is the most important part of light extinction in the canopy. In order to evaluate the option of *in-situ* comparison of heterogeneous canopies based on the absorbed portion of light received by the single layer of sun-exposed green leaves, we analyzed double-shot pairs of images taken from the "*Transmission*" and the "*Reflection"* perspectives of the experimental plots under a planned natural lighting condition (Fig.5A). This approach was developed under the isotropic scattering assumption. The idea was approximating the non-detected (absorbed) portion of light based on mean detected (sensed) parts of reflected and transmitted components. Therefore, using different color thresholding values, the "*Transmission*" and "*Reflection*" ROIs (ranges of interest) were extracted from each type of the images, and normalized color values (Sonnentag, 2011; and Wang *et al.*, 2013) were calculated using

mean RGBs of either type of ROI. We propose that each normalized color value with any given amount, can simultaneously be used in two separate kinds of normalization equations: the equation between normalized reflected, transmitted, and absorbed components of total incident (received) light in either band; and the basic equation between various bands of light in each component (e.g. the summation of normalized reflected red, green, and blue colors which equals 1; Fig. 5B, Fig. S8A, and Fig. S8B). This general rule is shown by mathematical demonstrations and also color identities.

Although we could use a simple MATLAB code for image segmentation in DLBE analyses, in order to monitor the whole process visually and more interactively, we used Fiji (http://fiji.sc/Fiji) for thresholding in HSB color system (Schindelin *et al.* (2012)). The thresholding ranges used for extracting the vivid green surfaces providing transmitted light in images of "*transmission perspective*", were 43-70, 110-255, and 211-255 for *hue*, *saturation*, and *brightness*, respectively. Similar ranges for extracting the green surfaces subjected to full sunlight in "*reflection perspective*" were 50-119, 0-255, and 143-246, respectively. Accordingly, we used the "*Image>Adjust>Color Threshold (default thresholding method)*" tool for making selections, and followed the "*Analyze>Color Histogram*" path for results. It is notable that (1) here we used HSB color system only for making selections, and results of color analyses –as individual means of color values- in the selected segments were produced in RGB system; (2) we can use alternative thresholding values or even methods for other types of canopies or conditions, provided that appropriate sampling i.e. choosing the pure defined areas (with strict selection) in either type of perspective is resulted.

2.3.3. An unexpected observation (background –soil- reflection)

As is described in the Results section, analyzing the *NOPOV* images, we also had an unexpected observation, for which, further evaluations were carried out (see the Results section). In the case of image background (soil) analyses, we used the non-vegetation parts in ST1 i.e. non-selected pixels by the thresholding method of Green>Red. For the evaluation conducted with the aim of refining background segmentation by reducing highly reflective surfaces, we limited the selection to the pixels with the color range of 1 to 244; so no selected pixel had higher color values for red, green, or blue (see the resulted segmentation in Fig. S9). Furthermore, we compared our new criteria with some available image-derived indices in literature provided for visible bands, in order to find the best one for predicting grain yield. Below is the list of these indices (Fig. S9M):

- $\%\text{Canopy Coverage(CC)} = \frac{\text{Number of vegetation pixels}}{\text{Total number of image pixels}} \times 100$ (8)
- $\text{G/R} = \frac{\text{Green value of vegetation}}{\text{Red value of vegetation}}$ (9)
- $G - R = \text{Green value of vegetation} - \text{Red value of vegetation}$ (10)
- $Normalized\ redness\ intensity$: $NRI_{veg} = \frac{Red_{veg}}{Red_{veg}+Green_{veg}+Blue_{veg}}$

  Veg: vegetation; similar formulae were also utilized for NGI_{veg} and NBI_{veg}.

  (11)
- $\text{VI}_{\text{green}} = \frac{Green-Red}{Green+Red}$ (12)
- $\text{SAVI}_{\text{green}} = (1+L)\frac{Green-Red}{Green+Red+L}$; L=0.5 (13)
- Triangular greenness index: (14)

  $TGI = -0.5[(670-480)(R_{670}-R_{550}) - (670-550)(R_{670}-R_{480})]$

  $R_{670}, R_{550}, R_{480}$ are reflectance in red, green, and blue bands, respectively, i.e.:

  $TGI = -0.5[(670-480)(Red-Green) - (670-550)(Red-Blue)]$.

Color indices of Canopy coverage (%CC), VI_{green}, and $\text{SAVI}_{\text{green}}$ are taken from Li *et al.*, 2010; G/R, G-R, NRI_{veg} and NGI_{veg} are taken from the paper by Wang *et al.*, 2013; and TGI is "triangular greenness index" (Hunt Jr., 2013).

All charts and figures were created and edited by Microsoft Excel 2013 and Adobe Photoshop CS6, comparison and reconciliation between images and thresholding (or segmentations) data were performed using Fiji, and Principal Component Analyses (in addition to casual equation evaluations) were carried out by XLSTAT Version 2016.02.28451 (Addinsoft).

3. Results

3.1. GSM: A new framework for evaluating light extinction in canopy

Using GSM model, in which vegetation parts were categorized into *n* dark to light groups based on green gradient, we observed that the individual increasing trends of red, green, and blue color mean values (from darkness to light, or oppositely, declining trend from light to darkness) were nonlinear and showed robust fit to exponential and/or polynomial equations (Fig. 1). This simple model was constructed based on the reflected light by the green canopy, and also includes the whole diverse detectable interactions of leaf surfaces with light, from

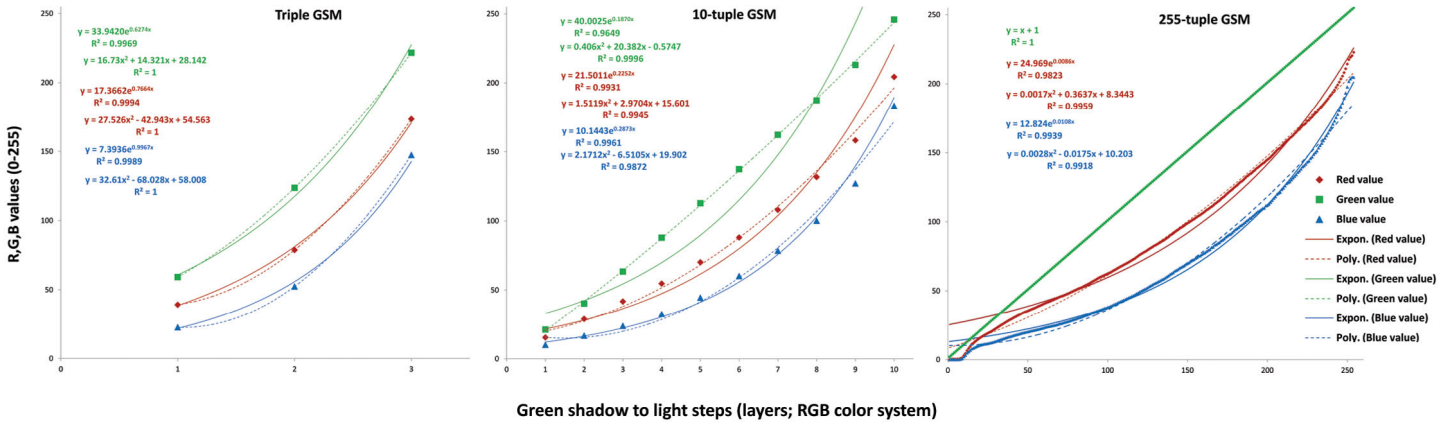

Figure 1. The concept and evolution of the Green-based Segmentation Model (GSM). The red and blue curves show robust exponential and/or polynomial attenuating trends. All the triple, 10-tuple, and 255-tuple GSMs are constructed based on similar number of vegetation pixels of an image taken from a monoculture canopy of "Chamran" wheat cultivar.

the very first exposures (by the highest intensities), to the minimal detected light in complete shadow which will soon be extinct completely (become non-detectable).

In order to evaluate the effect of the number of dark-to-light segments (groups) on consistency of equation coefficients, goodness of fitness, and hence determination of the best model type (among the simple forms of exponential, polynomial, and also power equations), a set of 3 images from three cultivars in monocultures at booting phase were analyzed, each for 3 to 10 segments (3- to 10-tuple GSMs, Fig. S1 B, and Table S1). Moreover, the model was run with a maximum possible number of 255 segments (255-tuple GSM) which simply implies plotting vegetation red and blue RGB colors against green, with the highest light resolution commercial digital cameras provide. Results indicated that although exponential and polynomial models were close competitors in either GSM with various number of segments (so that polynomial model was even slightly superior for red trend), the exponential model was the only one which had consistent coefficients over various GSMs (see respective C.V.s, Fig. S1 B).

Another comparison carried out between exponential and polynomial curve fittings for 255-tuple GSMs of 24 images taken from monoculture plots (in 6 replicates) also revealed similar evidences (Fig. S1 C): the fitness indicators (R^2 and RMSE) confirmed slightly higher degrees of polynomial fitness for red color compared with blue; whereas, exponential coefficients had the superior consistencies for both red and blue colors. We should clarify that such exponential (or even polynomial) trends are indeed, the extinction process of reflected light, i.e. the image of light to shadow gradient. In other words, while a typical canopy light sensor records the light intensity available in a particular space within the canopy, digital images of canopies record the reflected portions of various light intensities (projected from green surfaces with probably diverse reflection/or absorption behaviors). Here, we suggest that these exponential trends (i.e. gradients of reflected light in either band from shadow to light, or vice versa in the case of moving from lighter to darker parts of the canopy) may provide both theoretically and practically a direct definition of canopy light extinction; which is extremely easy to calculate, and is supported by a robust light sampling.

While low level segmented GSMs (e.g. the triple one) are also supported by the whole vegetation pixels of the image, and even may be more informative in describing the overall nonlinear extinction trend of green light, the most advanced 255-tuple model is capable of describe a very detailed process of reflected light variations in the canopy (Fig. 1). Evaluating

the comparative local slopes (differentiations) of red and blue trends relative to green, we distinguished 5 apparent parts on either red or blue curves, based on which, consequently another type of segmentation was carried out (segmentation type 3, ST3, i.e. GSM curve-based segmentation, Fig. 2). Reconciling these curve-derived segments to the images by thresholding (Fig. 2 and Fig. S2), the total vegetation parts were categorized briefly into (from light to shadow):

(i) Highly reflective green points in the full sunlight (the most horizontal-perpendicular- surfaces relative to the direction of "*radiation on the leaf which is then reflected to the camera*") with "non-stable relative slopes" above 1 on the curve which eventually approach the maximum declining rate (highest local slope) of the entire curve (Red_{4-5} and/or $Blue_{4-5}$);

(ii) The important segment of Red_{3-4}/or $Blue_{3-4}$ whose ever highest declining slope, begin to decrease regularly towards the lower limits of 1. This segment covers the variations of reflection from the sun-exposed surfaces with altering angles, from relatively more horizontal to vertical directions. Up to this point on the curve, the main part of attenuation of reflective light for red and blue colors occurs.

(iii) Partial shadow: the range of fluctuating relative local slopes around 1(frequent shifting of attenuating rates above and below the rate of green; Red_{2-3}/or $Blue_{2-3}$), which is mainly matched with the vegetation points under partial shadow (penumbra, Fig. 2A, and Fig. S2). It implies that under partial shadows, the red and blue lights are extinct (absorbed) almost with similar rates to green.

(iv) Complete shadow: the widest segment of the curve (Red_{1-2}/ or $Blue_{1-2}$, include the most diverse green values on the horizontal axis) with steadily declining relative slopes less than 1, i.e. less red and blue light extinction (absorption) compared with green (may also be comparable with the reported evidences for further penetration of green light into the leaf, as a particular micro-canopy; Sun *et al.*, 1998; Terashima *et al.*, 2009).

(v) Deep shadow: the darkest green part of the canopy in which the rest of red and blue lights are attenuated (absorbed) by higher rates compared with green (red and blue local slopes exceed again the constant slope of 1 for green, R_{0-1} or B_{0-1}). Finally, blue light intensity reaches a non-detectable reflection earlier than red on the curve, i.e. maybe less penetration to the deepest parts of the canopy (this may also be related to the higher wavelength of red color). We think that such precise

A

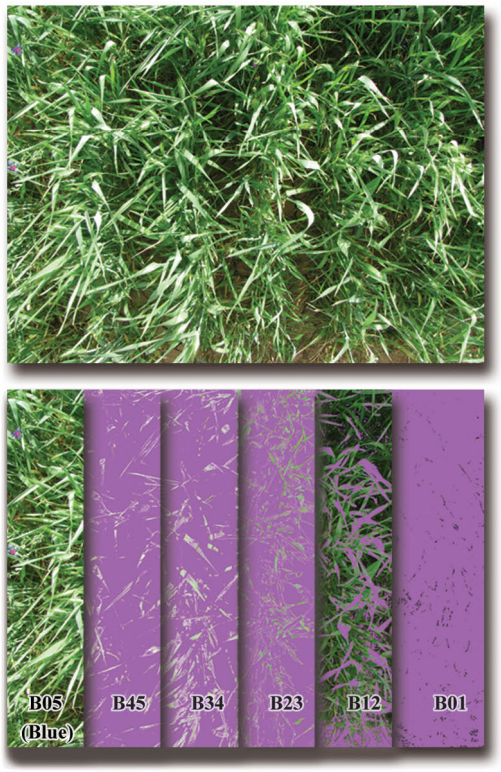

Figure 2. The curve-derived segmentation type 3 (ST3) for 255-tuple GSM, based on comparative attenuation rates (slopes) of red or blue reflected light relative to green. **(A)** Reconciling the blue curve segments to the image of a wheat canopy (monoculture of Chamran cultivar) using color thresholding. **(B)** The red and blue curves of 255-tuple GSM are segmented into 5 distinct parts, based on the relative changes in their local slopes compared with the green line. The color bars are reconstructed using the output values of 255-GSM, e.g. the "RGB" bar is made using the mean red, green, and blue values; the "R vs. G" bar indicates the actual attenuating trend of red color in 255-tuple GSM; and the "1:1 R" bar shows the conceptual attenuating trend of the red color, if it had been declined linearly as the same as the green line. **(C)** Comparative variations of the local slopes of the red and blue curves relative to the constant slope of the green line.

B

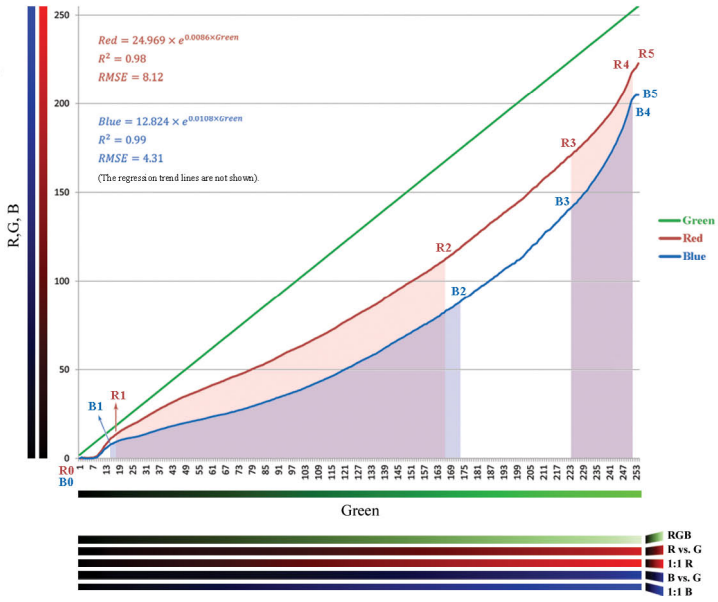

C

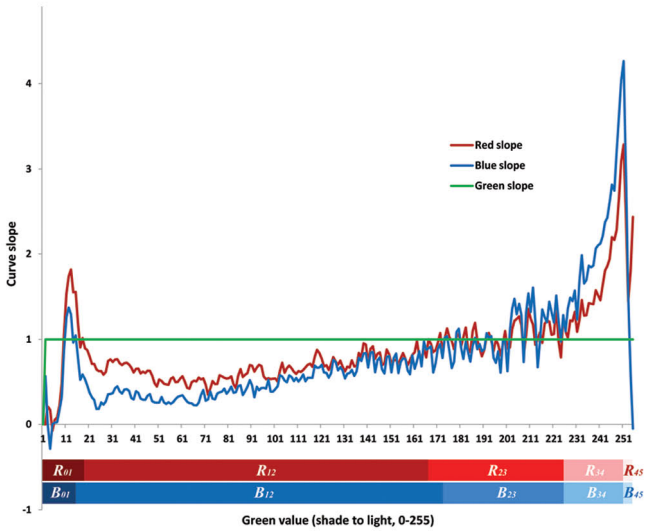

(fine) discriminations e.g. between partial and complete shadows in the canopy, are a reasonable confirmation of the efficiency of GSM and related ST3 in describing the entire features of reflected-light extinction in the canopy.

Afterwards, we defined more than 70 primary and 60 secondary curve characteristics (Table S2) by which the whole 15 treatments (in 6 replicates) were evaluated. We were also concerned about whether or not each characteristic or related phenomenon could be extrapolated to broader kinds of canopies (e.g. based on high or low probability values, respectively; see the Table S2 for complete results). A brief list of curve-derived indices and the most important findings are (Fig. 3, Fig. S3):

(a) In full sunlight, the main portions of reflected-red and -blue light attenuation are oppositely occur in the different classes of leaf surface angles, i.e. the declining rates of reflected red light were higher in the R_{4-5} segment (where the angles are shifting from the most horizontal surfaces to a little more slanted directions) compared with R_{3-4} (the segment including more slanted towards relatively perpendicular directions); while, the decreasing rate of reflected blue light in B_{3-4} is relatively higher than B_{4-5}. Obviously, two major reasons for declining trend of reflected light from horizontal to perpendicular angles are lower intensities of light received by non-horizontal surfaces, and also that the main direction of reflection from green surface, is diverted from vertical to other angles, so the light recorded by the camera is indeed, a scattered reflection beam (not the strongest projected in the main direction of reflection). We believe that the comparatively different declining trends of red and blue reflected light in similar segments (classes of angles) are evidences for the different effects of surface angle on red and blue extinction (and/or penetration into the leaf), i.e. the main portion of extinction for either kind of (red or blue) light occurs in a separate range of angles; the fact could also be extrapolated to some other kinds of canopies.

(b) Interestingly, the 15 mixture treatments were significantly different in relative red and blue extinction (absorption) under complete shadow (R_{1-2} and B_{1-2}), while, there were no other significant difference between treatments including segments under sunlight (except for Red_{4-5}). It is notable that the areas between green-red, or green-blue curves show the accumulated extinction (absorption) of related light compared with green (Fig. 3 C&D).

(c) The overall rate (linear slope) of either (red or blue) light extinction under complete shadow was almost equal to its inverse rate in full sunlight. However, we think that it is

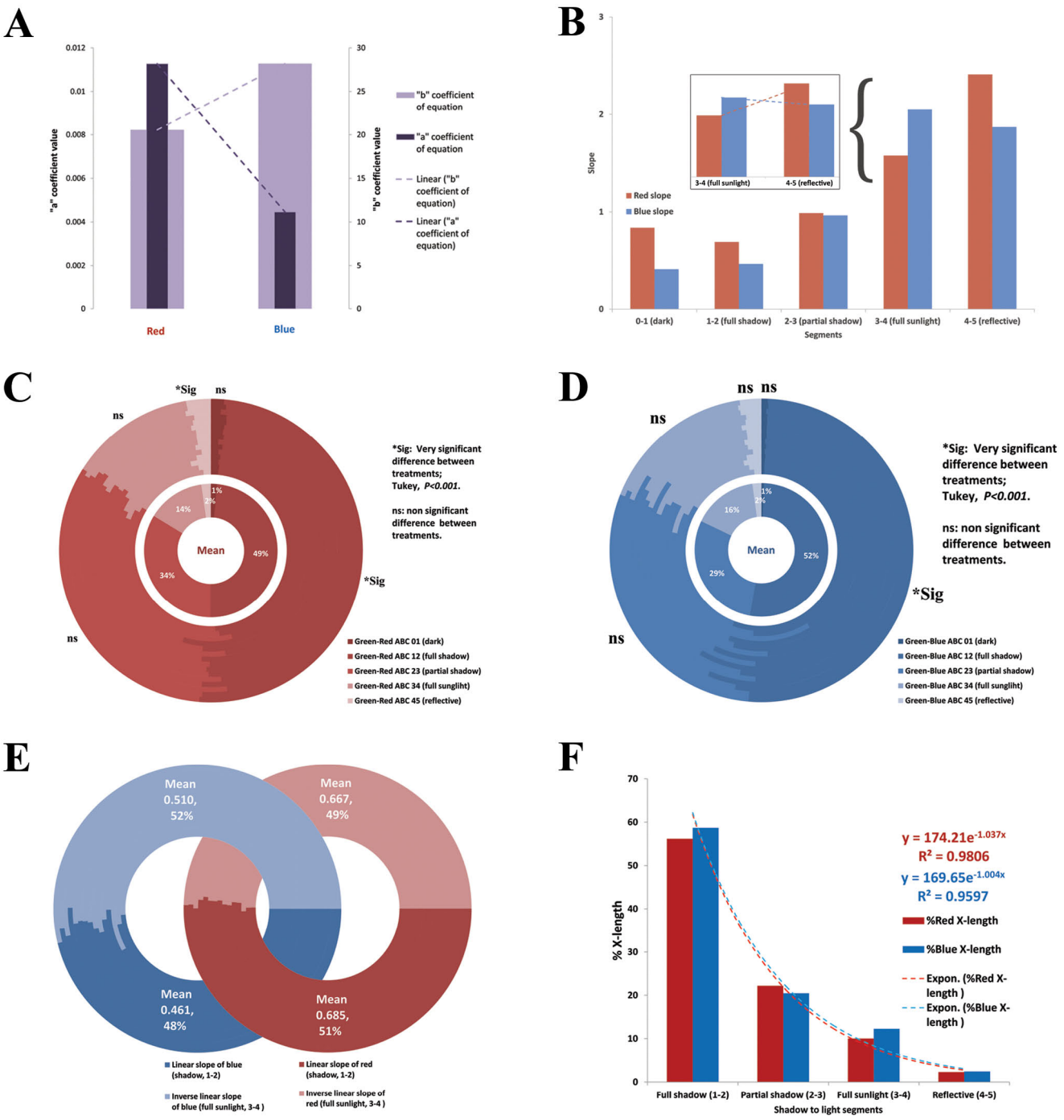

Figure 3. Several new aspects of light extinction in the canopy described using the curve characteristics of 255-tuple GSM. (A) the coefficients of exponential equations for red and blue light extinction (the overall mean values for 90 plots). **(B)** Comparing mean slopes of light extinction in "full sunlight" and "reflective" segments suggest that the maximum penetration rates of red and blue lights into the exposed leaves occur at different arrangement angles relative to sunlight (i.e. red and blue light are extinct by the green surfaces arranged relatively horizontal –perpendicular to sunlight-, and in a more slanted direction, respectively). **(C)** The area between the green and red curves (relative trapped or non-reflected red light) over the 15 treatments/90 plots. **(D)** The area between the green and blue curves (relative trapped or non-reflected blue light) over the 15 treatments/90 plots. **(E)** In the dense canopy of booting phase, the rate (linear slope) of the red or blue light extinction in shadow is almost equal to its inverse rate extinction under full sunlight condition. In the doughnut charts of the parts C to E: the 15 mixture treatments (i.e. 1, 2, 3, 4, 12, 13, 14, 23, 24, 34, 123, 124, 134, 234, and 1234) are arranged from center towards outside, respectively. "1" to "4" represent the early to middle ripening wheat cultivars, and each digit is a cultivar included in the mixture. **(F)** The x-lengths of the shadow to light segments of the red and blue curves (excluding the darkest segment of 0-1).

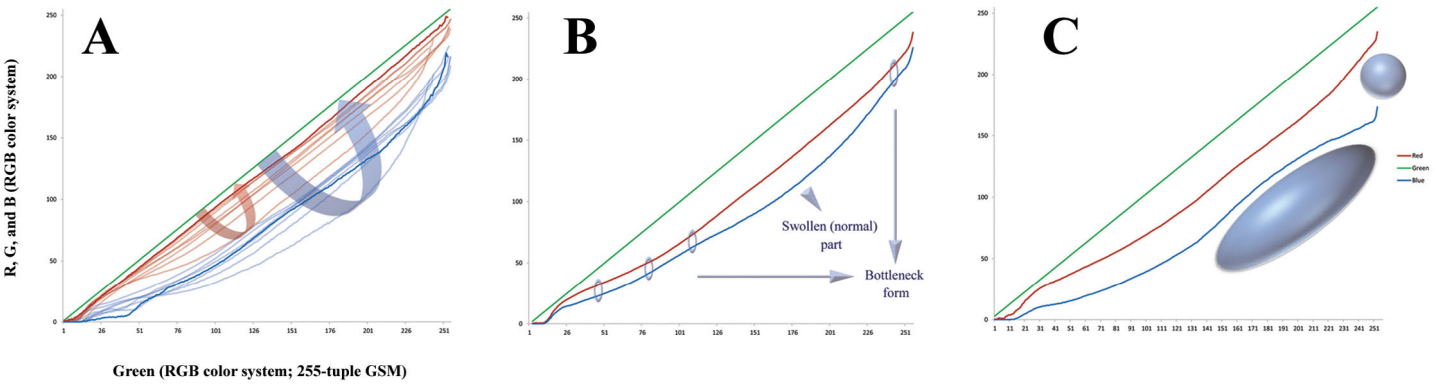

Figure 4. The effects of phenology and environmental stresses on 255-tuple GSM. The red and blue curves are affected by the canopy growth stage (phenology, **A**), water **(B)** and **(C)** cold stresses, whose diversion from the normal forms are indicated for the latter two as a bottleneck form or by ellipsoids.

limited to the condition of our experiment (booting phase of wheat), and further extrapolations require more investigations (Fig. 3E).

3.1.1 Effect of Phenology on light extinction trend

The 255-tuple GSM is sensible to phenological variations and hence, capable of determining relative growing stages (Fig. 4A, and Fig. S4), which despite many other introduced image-derived indices and methods, continues to detect the light extinction even late in the season (Fig. S5). Accordingly, from emergence, the overall areas between green-red and green-blue curves begin to increase until reaching their maximum values, with the most curvature form at the late tillering and early stem elongation phases, at the time when the most dense canopy has been formed due to intensive leaf production and low plant heights. Following stem elongation, increased canopy height lead to a returning trend, as towards the end of growing season -in particular- the red trend line again approaches to the green line.

3.1.2. Effects of water and cold stresses on light extinction trend

As shown in Fig. 4 B&C, Fig. S6, and Fig. S7, we observed that the light extinction was influenced by environmental stresses i.e. comparatively abnormal diverted forms mainly made by altered (either increased or decreased) reflection of blue light under sunlight to complete shadow conditions. We propose an acceptable diagnostic role for 255-tuple GSM in detecting various kinds of stresses which affect the light extinction, especially considering the total or partial variations of the area between blue-red and blue-green trend lines.

We emphasize that the exponential equation and/or fitness of GSM may be changed under stress and abnormal conditions, and also the general ST3 may be required to be carried out in a different way (e.g. segmenting the GSM curve into only two segments based upon having slopes either more or less than 1). However, GSM is so flexible to provide the opportunity for calculating such diversions compared with the typical form. Moreover, the 255-tuple GSMs for some other canopies (mostly included single plants as a newly defined canopy) and also for sunlight radiation (detected attenuating process before reaching the canopy) are represented in Fig. S10.

3.2. Double-shot light balance equations (DLBE): an approach for in-situ spectroscopy of single leaf-layer

Utilizing DLBE method, we observed briefly:

(a) reasonable comparative ratios of colors for non-detected (mainly absorbed) light (i.e. averaged over 15 treatments: 31.6%, 5.8%, and 62.6% for red, green, and blue, respectively, which seems not to be in conflict with the expected spectral behavior of the leaf; Fig. 5C);

(b) significant differences among treatments, which were recognized precisely, hence shows the reliability of the method for comparisons (see probability values and standard errors of the whole experiment in each comparison, Table 1); and eventually,

(c) while mixture treatments showed very significant differences in normalized absorbed (non-detected) green and blue lights, they were not statistically different in normalized absorbed red light (Table 1), which indicate that potential variations between treatments in light absorption by sun-exposed single layer of leaves was made by green and blue bands, rather than red.

3.3. Shade of grain yield on the soil

Analyzing the images of the booting phase, we unexpectedly observed a surprising phenomenon, in which the red color of the background (soil) was simulating the variation of final grain yield of such complex wheat canopies in a conservative manner (i.e. very precise mimicry of relative grain yield patterns for monocultures, and predicting the exact direction of fluctuations including curve minimum and maximum points over mixtures –with a minor exception for the case of treatment "*12*" to "*13*"-, Fig. 6 B, and Fig. S9). Notably, the basic condition which made this occurrence recognizable, was the natural lighting designed for the DLBE experiment (the imaging time i.e. 2 hours after solar noon, when almost the total under-canopy soil surface was covered by complete shadow); therefore, it is expected that the surface of homogenous, dry, and bare silty-clay soil with a relatively natural red tint, had strongly reflected the extinct sunlight –particularly in the red band- which had been filtered by the green canopy.

We carried out several analyses in order to further understand the process. First, we supposed that regardless of the band, this property might be related to the general intensity of overall instant illumination penetrated into the canopy (including red, green, blue, and maybe

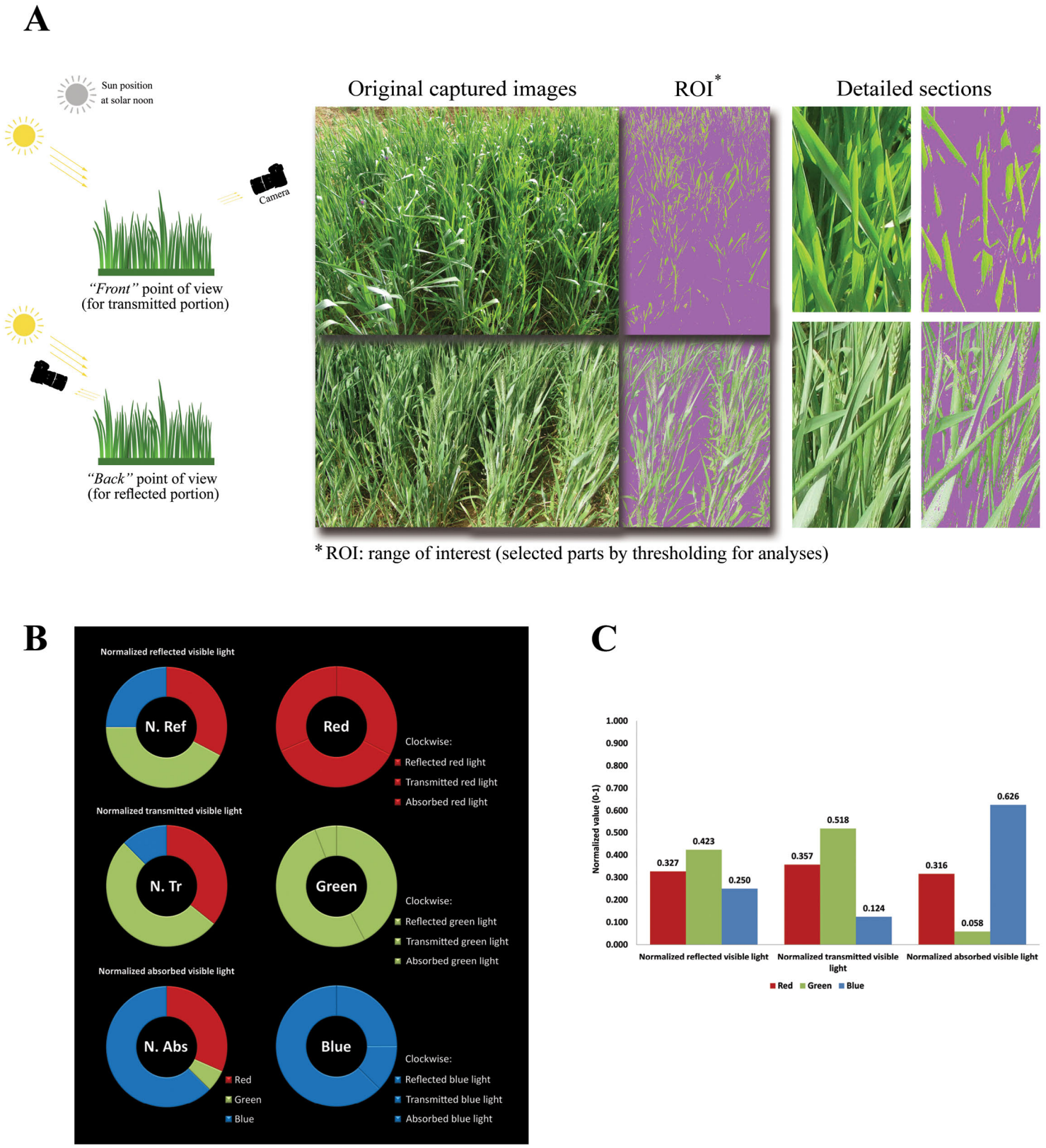

Figure 5. **The Double-Shot Light Balance Equations (DLBE) are introduced for an innovative in situ spectroscopy of the (sun-exposed) single leaf-layer, particularly in heterogeneous canopies. (A)** The schematic figure for imaging and determining ROIs (the purple area is the non-selected part). **(B)** The general concept of DLBE which is based on the simple fact that the normalized values of red, green, and blue lights in either reflecting, transmitting, or absorbing space may also be used interchangeably in the equations between the reflected, absorbed, and transmitted light of either band (consider the slices with the same color). **(C)** The results of DLBE for mixture treatments (the overall mean values over the 15 treatments/6 replicates).

Table 1. The results of DLBE (Double-shot Light Balance Equations) for the 15 cultivar mixture treatments.

Treatments	R_{front}	G_{front}	B_{front}	R_{back}	G_{back}	B_{back}	R absorbed ratio	G absorbed ratio	B absorbed ratio
1	0.358 a	0.514 b	0.128 a	0.330 a	0.428 a	0.241 d	0.311 a	0.058 bcde	0.631 abcd
2	0.357 a	0.513 b	0.130 a	0.328 ab	0.423 ab	0.249 abcd	0.315 a	0.063 abc	0.621 cde
3	0.358 a	0.513 b	0.129 a	0.327 abc	0.415 c	0.258 a	0.315 a	0.072 a	0.613 e
4	0.356 a	0.533 a	0.111 b	0.324 c	0.426 ab	0.250 abcd	0.320 a	0.041 f	0.639 a
12	0.359 a	0.521 ab	0.119 ab	0.329 ab	0.427 ab	0.244 cd	0.312 a	0.051 def	0.637 ab
13	0.358 a	0.513 b	0.129 a	0.328 ab	0.421 bc	0.251 abcd	0.313 a	0.067 ab	0.620 de
14	0.357 a	0.524 ab	0.119 ab	0.327 abc	0.427 ab	0.246 bcd	0.316 a	0.050 ef	0.634 abc
23	0.357 a	0.515 b	0.128 a	0.327 abc	0.421 abc	0.253 abc	0.316 a	0.064 abc	0.620 de
24	0.358 a	0.520 b	0.122 ab	0.326 bc	0.426 ab	0.248 bcd	0.315 a	0.054 cde	0.631 abcd
34	0.356 a	0.518 b	0.126 a	0.326 bc	0.420 bc	0.254 ab	0.318 a	0.062 abcd	0.620 cde
123	0.356 a	0.513 b	0.131 a	0.327 abc	0.423 ab	0.249 abcd	0.317 a	0.064 abc	0.620 de
124	0.357 a	0.517 b	0.127 a	0.327 abc	0.425 ab	0.248 abcd	0.316 a	0.059 bcde	0.625 bcde
134	0.355 a	0.519 b	0.126 a	0.325 bc	0.423 ab	0.252 abc	0.320 a	0.058 bcde	0.622 cde
234	0.357 a	0.522 ab	0.120 ab	0.325 bc	0.424 ab	0.251 abcd	0.318 a	0.054 cde	0.628 abcd
1234	0.357 a	0.520 b	0.123 ab	0.326 bc	0.421 abc	0.253 abc	0.317 a	0.059 bcde	0.624 bcde
Mean	0.357	0.518	0.124	0.327	0.423	0.250	**0.316**	**0.058**	**0.626**
P value	0.891	**0.000**	**0.000**	**0.000**	**0.000**	**0.000**	0.156	**0.000**	**0.000**
Std. Error	0.0004	0.0006	0.0006	0.0002	0.0004	0.0005	0.0005	0.0006	0.0007

The normalized red, green, and blue values of the three complementary forms of the reflected light (using the *reflection perspective*), transmitted light (using the *transmission perspective*), and the absorbed light (calculated by subtracting the two mentioned portions from the total input light value of 1). Treatments 1, 2, 3, 4,...,1234 are the mono- and mixed cropping of four early to midlle ripening wheat cultivars in 6 replicates, at the booting physiological phase. In each treatment, any single digit refers to a cultivar included in the mixture. The statistical comparisons are carried out using Tukey's test, $P < 0.05$.

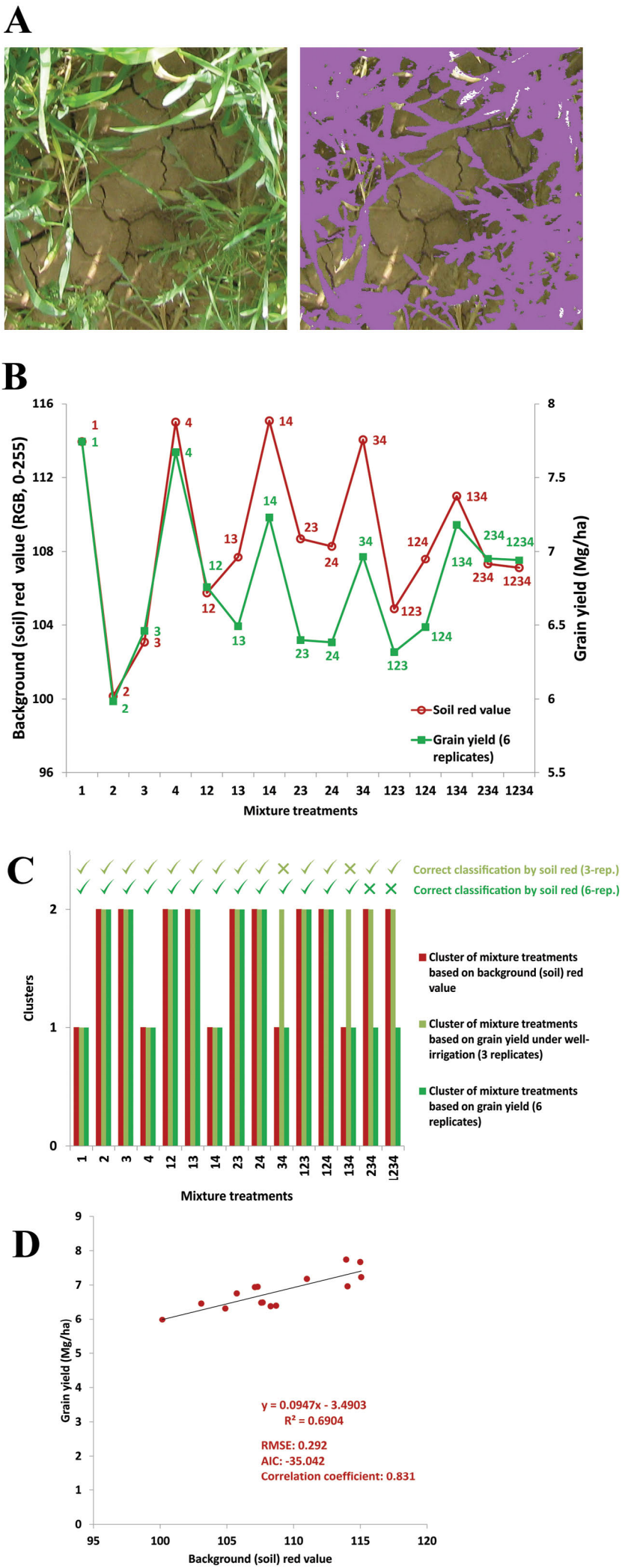

Figure 6. The red color of background (soil) reflects the relative pattern of grain yield even in the complex mixtures. (A) A slice of an image shows the result of color thresholding (segmentation type 1). **(B)** The comparative patterns of variation for background (soil) redness and grain yield over the mixture treatments. **(C)** The comparative clustering of mixture treatments based on the background (soil) redness, grain yield with 6, and 3 replicates. **(D)** The relationship between the background (soil) redness and grain yield (the linear trend line for regression is drawn).

mean RGB values of soil) rather than been only limited to the red color; for instance, due to less or more canopy openness. In addition to visual comparison of the similarities between patterns of grain yield and various light colors, we also examined indices by relationship measures (correlation and regression), and also based on how similar to grain yield they could cluster the treatments (k-means clustering). As shown in Fig. 6 and Fig. S9A-D, we found that although other bands and mean-RGB had some acceptable degrees of relationship or similarity with the grain yield trend, the red color was the best criterion. Considering ST1 (see Method section), beside soil points, the image background was also included high-reflective points of green leaves which did not show typical spectral behavior in the range of visible light (i.e. reflecting higher red intensities than green; so were not categorized as vegetation segments). Hence, applying additional thresholding, we tested these two parts i.e. highly reflective points and absolute soil parts separately (which on average were equal to 15.42% vs. 0.83% of total image area), but more interestingly, we found that the similarities and relationship with grain yield lowered considerably, in particular for mixtures (Fig. S9F-9J). We expected that the existence of numerous high-reflective points would probably imply that there were more horizontal leaf surfaces in the canopy which could eventually contribute to grain yield by absorbing sunlight at higher/more efficient rates; the idea was rejected, and the reason remained undiscovered for us as to how inclusion of the described high-reflecting points (with relatively very limited area and steady values) in image background, may improve the relationship and similarities. Additionally, since 3 out of 6 replicates were later exposed to water stress after anthesis, we repeated the analyses excluding grain yield values of deficit-irrigated treatments (i.e. 45 plots). Again despite our expectations, this reasonable strategy did not improve the condition, which shows the importance of a greater number of replications in the tradeoff with reduced variations among the treatments (Fig. S9K). Finally, we compared the background (soil) red values with other image-derived indices available in literature for probable ability in predicting grain yield patterns (although there was not any claim for their relationship with grain yield, they were the only available criteria in this context). This comparison also suggested background red values as the best index for predicting relative pattern of grain yield, if not the unique one (Fig. S9M).

4. Discussion

Using the often ignored capability of digital cameras in rigorous light sampling, and based on relative quantities, we observed that the green-scaled bidirectional reflectance from the canopy has a robust exponential attenuation gradient, which can be directly utilized for

identifying and characterizing canopies. In other words, the whole variation in reflected light caused by diverse phenomena including angle shifting of sun-exposed leaf surfaces, or partial to complete shading, may be thoroughly represented in only a simple equation. Besides, a curve-based segmentation (ST3) of high level GSM (i.e. 255-tuple) may describe precisely the entire detectable interactions of light in a canopy. We have categorized and reported these processes in five distinct classes. Moreover, evaluating considerable curve characteristics provided us with new valuable criteria for comparing the optics of different canopies. Utilizing such criteria, we also reported several aspects of light extinction in canopies, e.g. evidences for the fact that the main portions of red and blue light extinction occur in different angles, or canopies may be significantly different in light interactions under complete shadow. Potential diagnostic roles of GSM are also demonstrated.

We believe that now we can describe the canopy light extinction (and consequently canopy properties) in a direct representation, independent of LAI concept. Accordingly, a canopy may be defined simply by equations of its GSM curves, as any collection of vegetation surfaces that provides a light gradient. For instance, depending on purposes (once segmented from background i.e. ST1), we can consider a rolled leaf that casts a shadow on itself as an individual canopy, since it provides a light gradient, which also may be comparable with a wheat canopy or even with a forest in a satellite image (although such given canopies may have qualitatively similar light gradients -i.e. light extinction equations-, they are different in tempo-spatial scales in which the identical light gradients are provided). Furthermore, canopy depth (and/or layer) is indeed an optical term (i.e. relatively reduced light intensity) instead of being a spatial concept; because green surfaces may be completely subjected to either sun or shadow at any height in the canopy. We propose the GSM model as a novel tool for widespread utilization of these applicable definitions, which seems to evaluate and describe vegetation stands more efficiently. Besides, the GSM model may contribute to measurement of radiation field and quantifying the scattering processes inside vegetation canopies, and also may be used for thresholding in segmentation of the vegetation parts based on the sun exposure (Fig. S2). Indeed, the GSM model indicates the relative trend of variations in red and/or blue bidirectional reflectance, against the linear increase of the sun exposure (with the slope equal to 1).

Additionally, we attempted to approximate a kind of applicable spectroscopy of the single leaf-layer in the canopy based on normalized detected components of transmitted and

reflected light, whose results show significant differences between canopies in absorption of green and blue light, and proposed some general rules based on DLBE.

Methodologically, it is notable about the DLBE evaluation that measuring the absolute quantities of absorption by single leaf-layer of such heterogeneous canopies either using destructive methods or sensor networks (if possible), requires theoretically considerable homogenous leaf/spot samplings and reasonable calculations. Even in methods utilizing image processing, the exact estimation of absolute light absorbed by single-leaf layer of a canopy needs sophisticated models established based on different assumptions about leaf optical properties (e.g. opaque vs. semi-translucent property of leaf, or isotropic vs. anisotropic scattering; Salisbury *et al.*, 1987; Dickinson, 2008; Terashima *et al.*, 2016). Our assessment was based on the isotropic assumption of radiation scattering and also normalized values, which seem to meet the preconditions for comparisons among the mixtures (instead of measuring the absolute quantities). To the best of our knowledge, there is no alternative method for *in-situ* estimation of light absorption by the single-leaf-layer of the heterogeneous canopies.

Eventually, we reported an accidental observation in which the red color level of the image background (soil) in the booting phase could simulate and predict the relative pattern of the final grain yield, even in complex canopies. It seems that this index may be utilized for grain yield prediction at least in wheat canopies, a fact that shows the potential importance of reflections from the usually neglected part of canopies, i.e. non-vegetation (mainly soil) in image processing and remote sensing approaches.

It is notable that the present study aimed comparing canopies of cultivar mixtures (under the particular conditions described, e.g. the zenith angel, camera model, genotypes and mixtures, etc.) based on their optical aspects suggested by image mining approaches and relative quantities; therefore, -except for the suggested reproducible methodologies- any extrapolation or generalization of the observations into other conditions requires further evaluations (especially when the absolute quantities in physical level are intended). Indeed, for agronomic purposes, we have statistically compared the mixture canopies with their corresponding monocultures (as the biological reference panels for reflectance), and there is no claim about the absolute quantities. Furthermore, here, an alternative image-based representation of light extinction is proposed. This framework can neither be compared to, nor validated by the conventional approaches in which the incident light within the canopy

spaces is measured. Instead, the results of the novel method may be validated using other types of (optical or spectral) cameras.

5. Conclusion

In the present study, we have evaluated novel computation methods for analyzing the images of heterogeneous wheat canopies. In order to monitor and visualize the reflected light gradient, an image-derived model (GSM) is introduced, which can identify crop (and also other) canopies in the form of one or two simple equations. The high-level version (i.e. 255-tuple) of GSM may provide detailed light interactions within canopies. Using this model, we have reported some aspects of canopy-light interactions for the first time. Moreover, the potential advantages of using digital cameras for a kind of in-situ spectroscopy of (even heterogeneous) canopies based on normalized RGB color values are indicated.

An accidental observation also revealed that the red color of the vegetation background (mainly soil), may predict and simulate the grain yield pattern at booting stage; a phenomenon that suggests non-vegetation parts may be included in canopy remote sensing and image processing techniques. We believe that our findings and new definitions as well as novel simplified methodologies used, may improve our knowledge of light extinction in canopy.

Acknowledgements

The authors wish to thank Shiraz University for providing field experiment facilities. Mr. Saeid Jafarizadeh is gratefully acknowledged for his contribution in writing MATLAB codes. The authors would also thank anonymous reviewers for their valuable comments and suggestions on a previous version of the manuscript.

References

Bauer, J., Siegmann, B., Jarmer, T. and Aschenbruck, N., 2016. On the potential of Wireless Sensor Networks for the in-situ assessment of crop leaf area index. Computers and Electronics in Agriculture, 128: 149-159.

Behera, S.K., Srivastava, P., Pathre, U.V. and Tuli, R., 2010. An indirect method of estimating leaf area index in Jatropha curcas L. using LAI-2000 Plant Canopy Analyzer. Agricultural and Forest Meteorology, 150(2): 307-311.

Casadesús, J. et al., 2007. Using vegetation indices derived from conventional digital cameras as selection criteria for wheat breeding in water-limited environments. Annals of Applied Biology, 150(2): 227-236.

Dickinson, R.E., 2008. Determination of the multi-scattered solar radiation from a leaf canopy for use in climate models. Journal of Computational Physics, 227(7): 3667-3677.

Easlon, H.M. and Bloom, A.J., 2014. Easy Leaf Area: Automated digital image analysis for rapid and accurate measurement of leaf area. Applications in Plant Sciences, 2(7): apps.1400033.

Glatthorn, J. and Beckschäfer, P., 2014. Standardizing the Protocol for Hemispherical Photographs: Accuracy Assessment of Binarization Algorithms. PLOS ONE, 9(11): e111924.

Gower, S.T., Kucharik, C.J. and Norman, J.M., 1999. Direct and Indirect Estimation of Leaf Area Index, fAPAR, and Net Primary Production of Terrestrial Ecosystems. Remote Sensing of Environment, 70(1): 29-51.

Hunt Jr, E.R. et al., 2013. A visible band index for remote sensing leaf chlorophyll content at the canopy scale. International Journal of Applied Earth Observation and Geoinformation, 21: 103-112.

Jacquemoud, S. et al., 2009. PROSPECT + SAIL models: A review of use for vegetation characterization. Remote Sensing of Environment, 113, Supplement 1: S56-S66.

Jonckheere, I. et al., 2004. Review of methods for in situ leaf area index determination: Part I. Theories, sensors and hemispherical photography. Agricultural and Forest Meteorology, 121(1–2): 19-35.

Lee, K.-J. and Lee, B.-W., 2013. Estimation of rice growth and nitrogen nutrition status using color digital camera image analysis. European Journal of Agronomy, 48: 57-65.

Li, Y., Chen, D., Walker, C.N. and Angus, J.F., 2010. Estimating the nitrogen status of crops using a digital camera. Field Crops Research, 118(3): 221-227.

Liu, J. and Pattey, E., 2010. Retrieval of leaf area index from top-of-canopy digital photography over agricultural crops. Agricultural and Forest Meteorology, 150(11): 1485-1490.

McCree, K.J., 1972. Test of current definitions of photosynthetically active radiation against leaf photosynthesis data. Agricultural Meteorology, 10: 443-453.

Monsi, M. and Saeki, T., 2005. On the Factor Light in Plant Communities and its Importance for Matter Production. Annals of Botany, 95(3): 549-567.

Munier-Jolain, N.M., Guyot, S.H.M. and Colbach, N., 2013. A 3D model for light interception in heterogeneous crop:weed canopies: Model structure and evaluation. Ecological Modelling, 250: 101-110.

Omasa, K., Hosoi, F. and Konishi, A., 2006. 3D lidar imaging for detecting and understanding plant responses and canopy structure. Journal of Experimental Botany, 58(4): 881-898.

Perot, T., Mårell, A., Korboulewsky, N., Seigner, V. and Balandier, P., 2017. Modeling and predicting solar radiation transmittance in mixed forests at a within-stand scale from tree species basal area. Forest Ecology and Management, 390: 127-136.

Razzaghi, F. and Sepaskhah, A.R., 2012. Calibration and validation of four common ET0 estimation equations by lysimeter data in a semi-arid environment. Archives of Agronomy and Soil Science, 58(3): 303-319.

Sakamoto, T. et al., 2012. An alternative method using digital cameras for continuous monitoring of crop status. Agricultural and Forest Meteorology, 154–155: 113-126.

Salisbury, J.W., Milton, N.M. and Walsh, P.A., 1987. Significance of non-isotropic scattering from vegetation for geobotanical remote sensing. International Journal of Remote Sensing, 8(7): 997-1009.

Schindelin, J.e.a., 2012. Fiji: an open-source platform for biological-image analysis. Nature methods 9(7): 676-682.

Shahrokhnia, M. and Sepaskhah, A., 2013. Single and dual crop coefficients and crop evapotranspiration for wheat and maize in a semi-arid region. Theoretical and applied climatology, 114(3-4): 495-510.

Sonnentag, O. et al., 2011. Tracking the structural and functional development of a perennial pepperweed (Lepidium latifolium L.) infestation using a multi-year archive of webcam imagery and eddy covariance measurements. Agricultural and Forest Meteorology, 151(7): 916-926.

Sun, J., Nishio, J.N. and Vogelmann, T.C., 1998. Green Light Drives CO2 Fixation Deep within Leaves1. Plant and Cell Physiology, 39(10): 1020-1026.

Terashima, I., Fujita, T., Inoue, T., Chow, W.S. and Oguchi, R., 2009. Green Light Drives Leaf Photosynthesis More Efficiently than Red Light in Strong White Light: Revisiting the Enigmatic Question of Why Leaves are Green. Plant and Cell Physiology, 50(4): 684-697.

Terashima, I., Ooeda, H., Fujita, T. and Oguchi, R., 2016. Light environment within a leaf. II. Progress in the past one-third century. Journal of Plant Research, 129(3): 353-363.

Viña, A., Gitelson, A.A., Nguy-Robertson, A.L. and Peng, Y., 2011. Comparison of different vegetation indices for the remote assessment of green leaf area index of crops. Remote Sensing of Environment, 115(12): 3468-3478.
Viña, A., Gitelson, A.A., Nguy-Robertson, A.L. and Peng, Y., 2011. Comparison of different vegetation indices for the remote assessment of green leaf area index of crops. Remote Sensing of Environment, 115(12): 3468-3478.
Wang, Y., Wang, D., Zhang, G. and Wang, J., 2013. Estimating nitrogen status of rice using the image segmentation of G-R thresholding method. Field Crops Research, 149: 33-39.

Watson, D.J., 1947. Comparative Physiological Studies on the Growth of Field Crops: I. Variation in Net Assimilation Rate and Leaf Area between Species and Varieties, and within and between Years. Annals of Botany, 11(1): 41-76.

Weiss, M., Baret, F., Smith, G.J., Jonckheere, I. and Coppin, P., 2004. Review of methods for in situ leaf area index (LAI) determination: Part II. Estimation of LAI, errors and sampling. Agricultural and Forest Meteorology, 121(1–2): 37-53.

Welles, J.M. and Cohen, S., 1996. Canopy structure measurement by gap fraction analysis using commercial instrumentation. Journal of Experimental Botany, 47(9): 1335-1342.

Xue, H. et al., 2015. Spatial distribution of light interception by different plant population densities and its relationship with yield. Field Crops Research, 184: 17-27.

Yao, H., Zhang, Y., Yi, X., Zhang, X. and Zhang, W., 2016. Cotton responds to different plant population densities by adjusting specific leaf area to optimize canopy photosynthetic use efficiency of light and nitrogen. Field Crops Research, 188: 10-16.

Zhao, F. et al., 2011. Measuring effective leaf area index, foliage profile, and stand height in New England forest stands using a full-waveform ground-based lidar. Remote Sensing of Environment, 115(11): 2954-2964.

Zou, X. et al., 2014. Photographic measurement of leaf angles in field crops. Agricultural and Forest Meteorology, 184: 137-146.

A

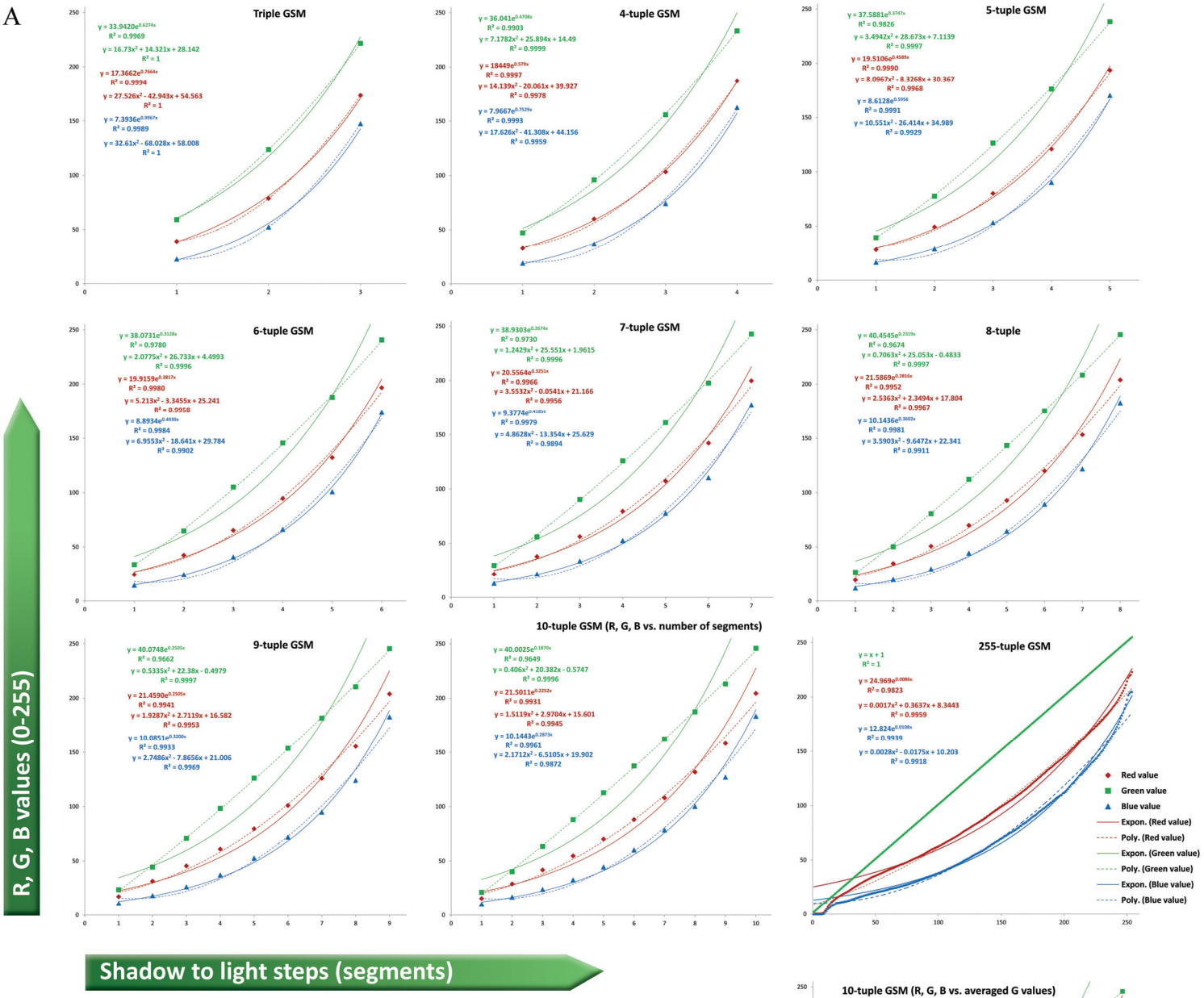

B

Comparative variations of coefficients for polynomial and exponential equations, GSM.

Sample	Layers	Red					Blue				
		Polynomial			Exponential		Polynomial			Exponential	
		a (poly.)	b (poly.)	c (poly.)	a (exp.)	b (exp.)	a (poly.)	b (poly.)	c (poly.)	a (exp.)	b (exp.)
1	10	0.0020	0.2727	13.1587	25.3684	0.008591	0.0031	-0.1133	15.4685	12.9461	0.010800
	255	0.0017	0.3603	7.9823	24.9691	0.008638	0.0028	-0.0231	10.2233	12.8241	0.010797
2	10	0.0018	0.3559	11.7923	27.3649	0.008493	0.0032	-0.0667	12.1269	13.3582	0.011018
	255	0.0016	0.4098	7.8354	27.0223	0.008532	0.0031	-0.0221	8.5973	13.2869	0.011020
3	10	0.0016	0.3741	7.4562	24.8352	0.008589	0.0028	-0.0444	8.3299	11.0067	0.011308
	255	0.0019	0.2842	12.5383	25.1945	0.008558	0.0032	-0.1333	13.1358	11.0286	0.011364
1	C.V. of 10 and 255	12.5052	19.5660	34.6269	1.1218	0.3811	8.2016	-93.5088	28.8723	0.6694	0.0197
2		6.5767	9.9542	28.5096	0.8910	0.3241	2.8277	-71.0926	24.0856	0.3783	0.0143
3		14.0975	19.3010	35.9461	1.0155	0.2559	8.5218	-70.7350	31.6624	0.1407	0.3467
Mean C.V.		11.0598	16.2737	33.0275	***1.0094***	***0.3204***	6.5170	-78.4454	28.2068	***0.3961***	***0.1269***

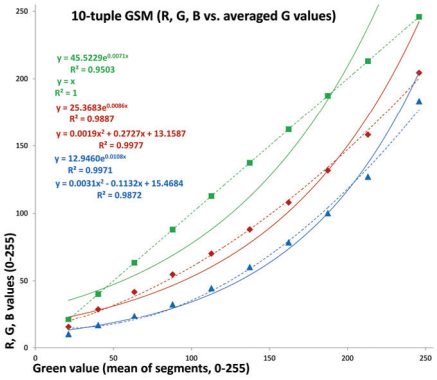

C

Comparison of exponential and polynomial models for 255-tuple GSM in four monocultures of wheat cultivars (with 6 replicates).

Cultivars	Consistency of coefficients among replicates of a single cultivar (coefficient of variation, %C.V.)										Goodness of fitness (R^2 and RMSE averaged over replicates of each cultivar)							
	Exponential (red)		Polynomial (red)			Exponential (blue)		Polynomial (blue)			Exponential (red)		Exponential (blue)		Polynomial (red)		Polynomial (blue)	
	b coeff.	*a* coeff.	x^2 coeff.	*x* coeff.	Constant	*b* coeff.	*a* coeff.	x^2 coeff.	*x* coeff.	Constant	R^2	RMSE	R^2	RMSE	R^2	Poly. Red RMSE	B R^2	B RMSE
1	2.842242	6.062613	14.75875	11.05724	8.282532	2.909595	10.42653	3.661675	42.22079281	9.316109	0.977036	9.201255	0.994802	3.743326	0.995735	3.839738529	0.989462419	5.152881425
2	2.980015	6.363184	14.82473	13.03087	38.96945	2.690594	9.137798	10.79274	88.67124038	40.3738	0.978714	8.855079	0.994862	3.807087	0.995356	4.013751066	0.99092375	4.968749335
3	1.942587	3.895648	14.74602	9.836061	14.49161	1.972454	7.783508	2.808954	45.24099172	12.54156	0.97608	9.859379	0.994332	4.551637	0.996347	3.668294207	0.99524384	3.878802089
4	2.747959	6.519684	18.04506	15.85442	20.00396	2.08405	5.87855	7.170945	47.40564927	20.73622	0.977735	8.816504	0.991632	4.55033	0.993608	4.575723614	0.983548832	6.369765135

The formulas of exponential and polynomial (quadratic) equations used are the simple forms of $y=ae^{bx}$ and $y=ax^2+bx+c$, respectively; e.g. for red color: $Red=a.e^{b.Green}$ and $Red=a(Green)^2+b(Green)+C$.

Fig. S1. Comparison of exponential and polynomial equations for various Green-based segmentation models (GSMs). (A) Triple to 10-, and 255-tuple GSMs for a single plot (monoculture of cultivar 1, see SI. 1 for extended data). **(B)** Variations of polynomial and exponential coefficients from 10-tuple to 255-tuple GSM. It is notable that the equation coefficients used in the table of this part are related to regressions between red/or blue colors and mean green values of segments, while the equations of the charts of 3- to 10-tuple GSMs in part (a) are for the relationship between each color and number of steps (segments, i.e. 3, 4,..., 10). **(C)** Comparison of exponential and polynomial models for 255-GSMs of replicated monocultures.

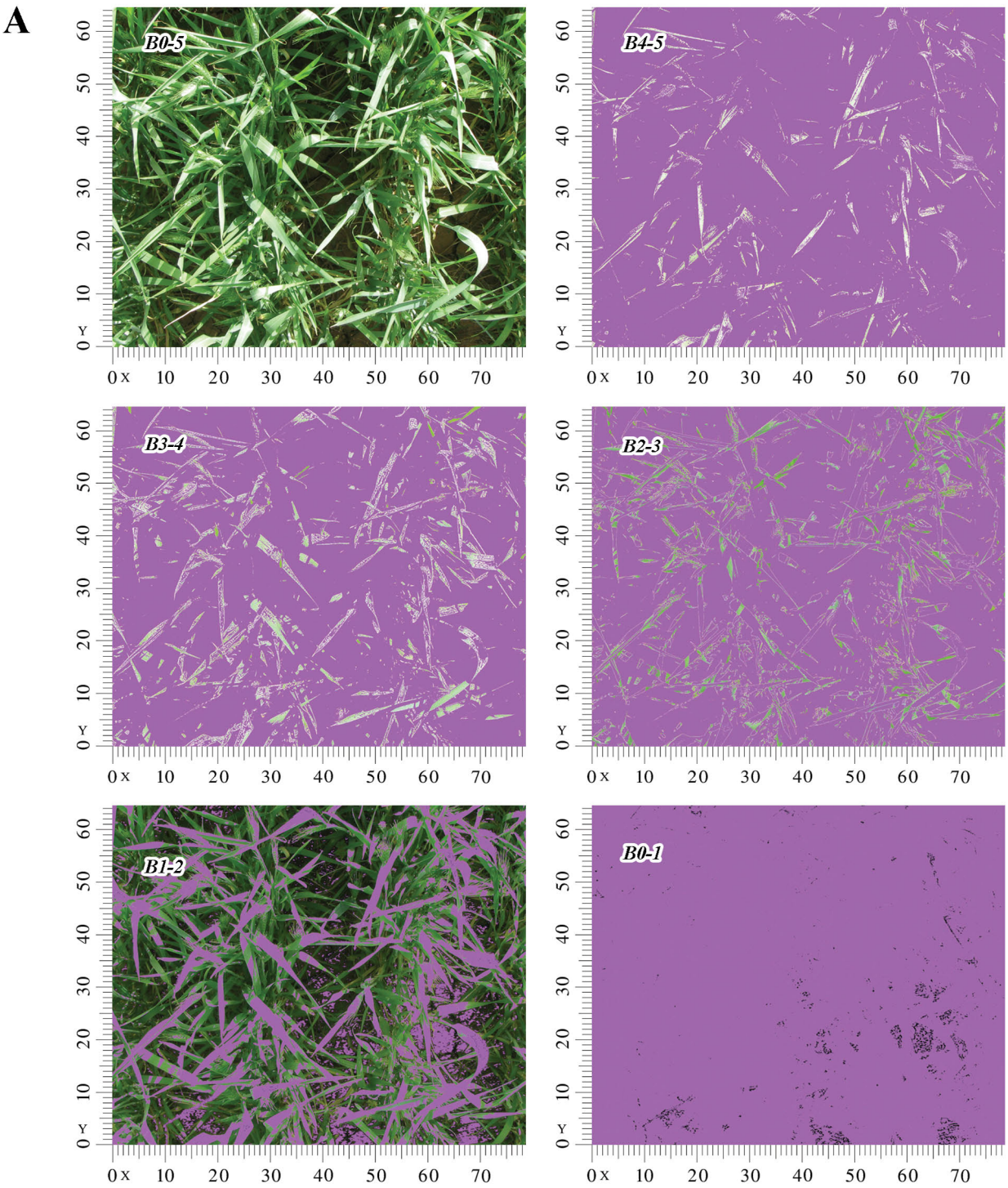

Fig. S2. Segmentation type 3 (ST3) for the image of a wheat canopy at booting stage. (A) and (B) The central section of an image (B0-5) segmented based on ST3 of the blue curve (depending on altering rate of blue light attenuation relative to green). In each photo, the purple mask has covered the non-selected pixels. Please note that, for example, the shadow on the leaf in the position (x=28, y=26) with the three parallel strips of shadows on the leaf at (x=10, y=15). The first one is categorized as a partial shadow, since it is observable in the segment B2-3 (where the blue light is attenuating almost with the same rate as green), while, the second set is identified as complete shadow (B1-2, i.e. blue light is attenuating with lower rates compared with green). Similarly, we can track different parts of any single rolled or folded leaf in various segments. Notably, (i) non-vegetative pixels are excluded previously by the segmentation type 1 (ST1), and (ii) the 5 segments represented here are complementary to each other, so each pixel may be included only in one segment.

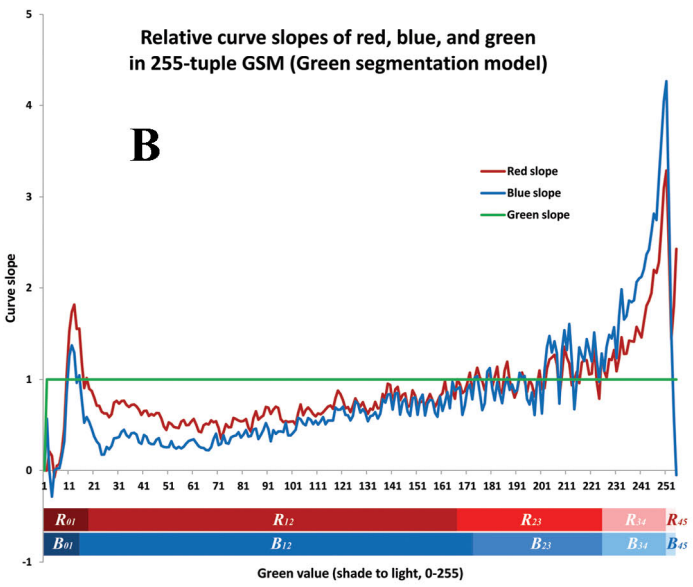

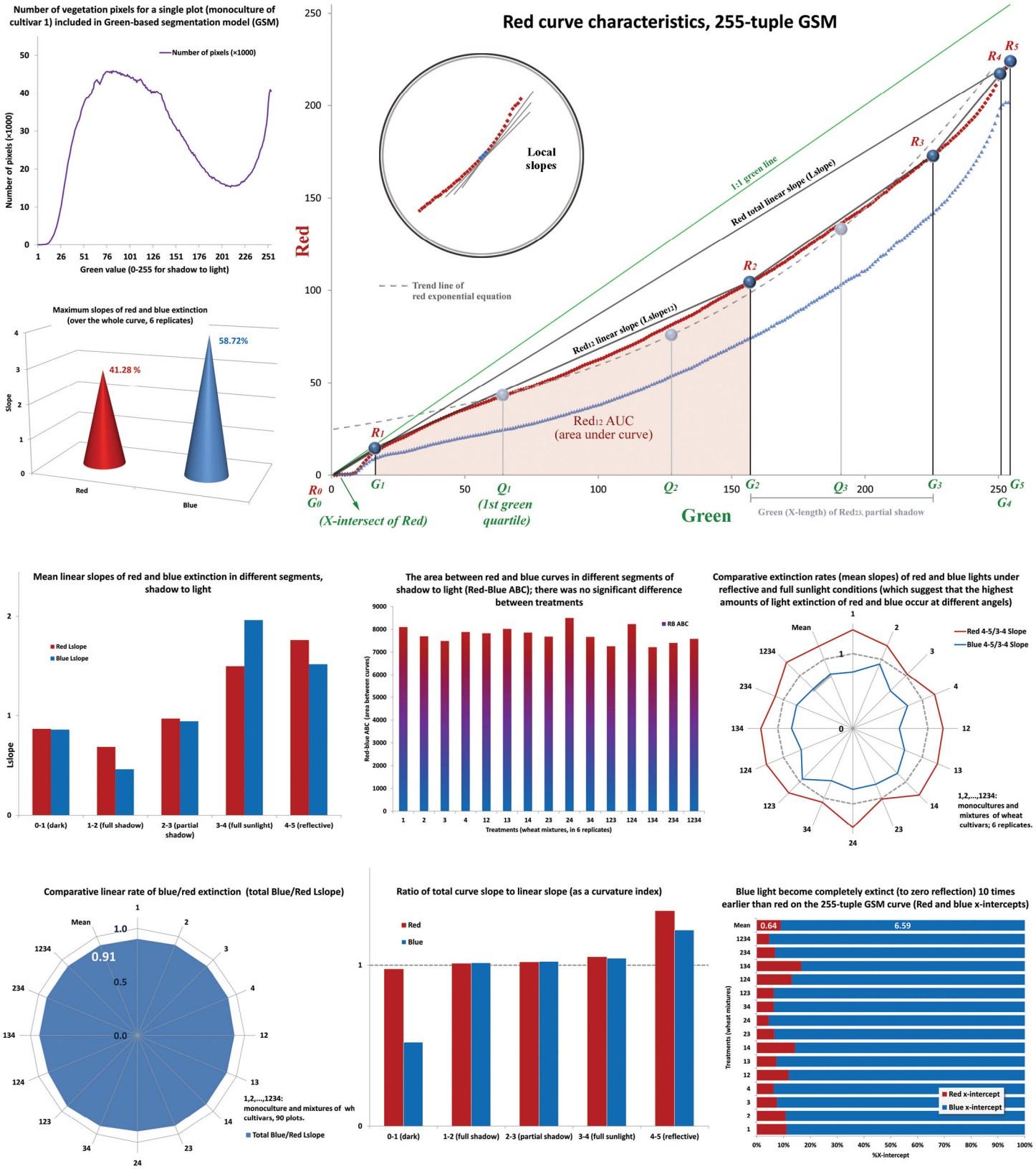

Fig. S3. Curve characteristics of Green-based Segmentation Model (GSM) including primary (directly calculated) and secondary (additionally processed) criteria, and several aspects they reveal. Such indices may be utilized for comparing canopies and studying general or exclusive interactions of light. Treatments (1, 2, 3, 4, 12, 13, 14, 23, 24, 34, 123, 124, 134, 234, 1234) are 15 mono- and mixed cropping of wheat cultivars in 6 replicates (1 to 4 are early to middle ripening cultivars, and each digit is a cultivar included in the mixture).

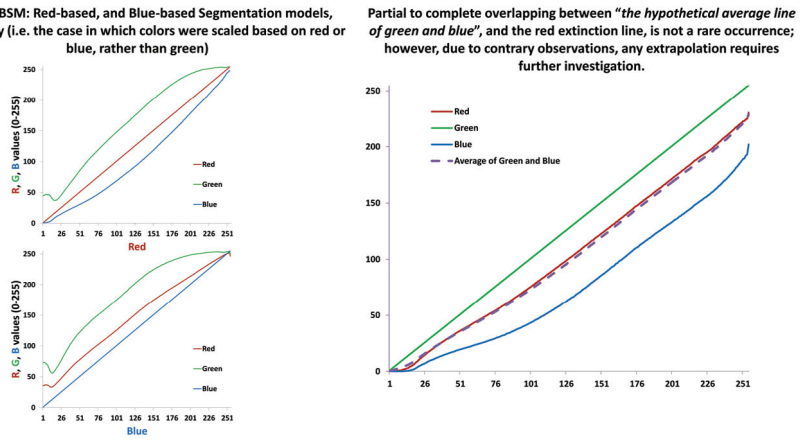

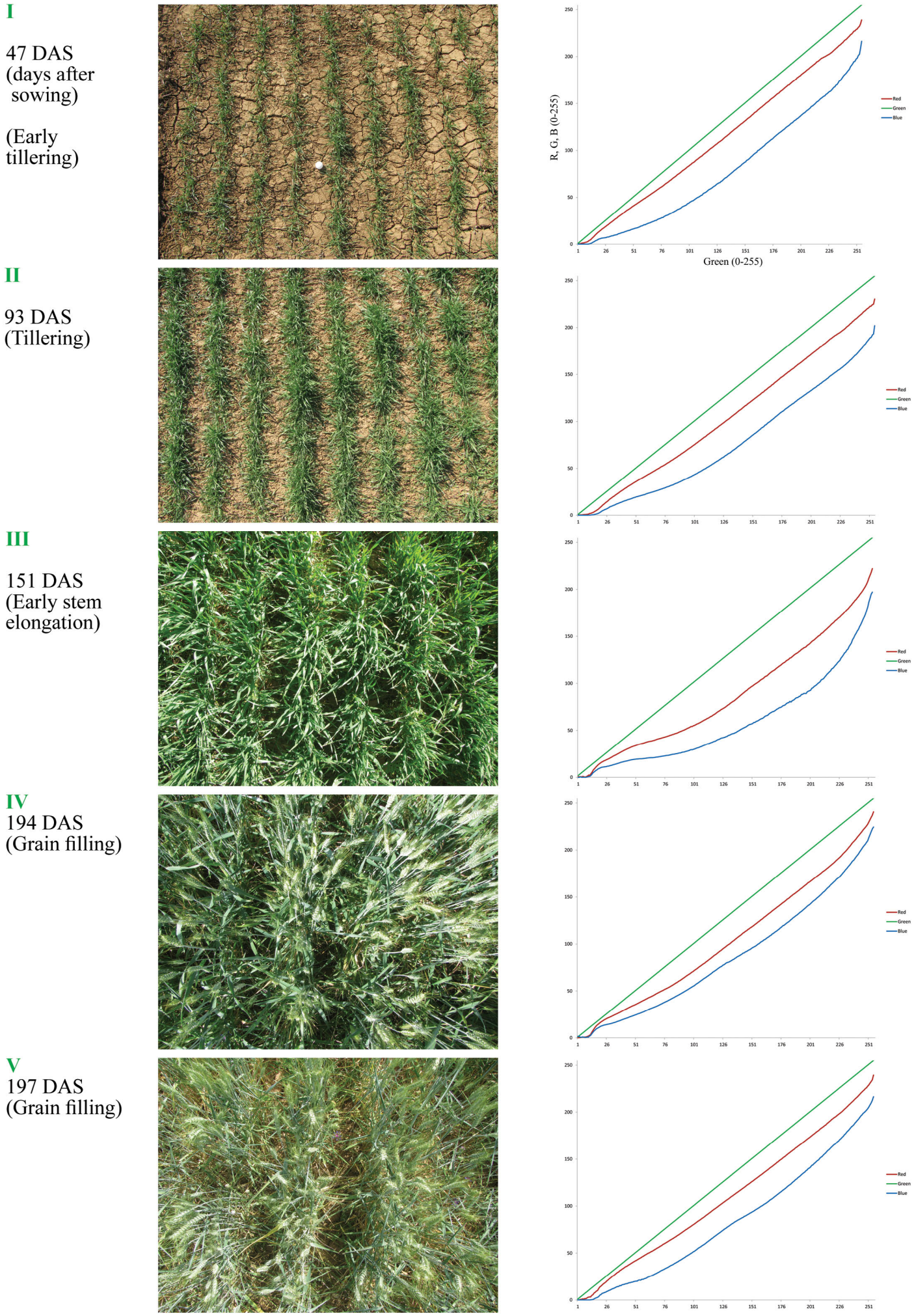

Fig. S4. Effect of growth stage on light attenuation in a green monoculture canopy. Considering the trends of red and blue lights relative to green, with the highest degrees of curvature at stage (III) due to highest canopy density.

A

VI
208 DAS
(Late physiological ripening)

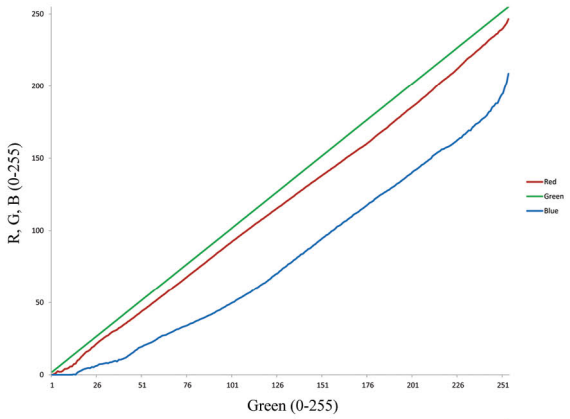

VII
211 DAS

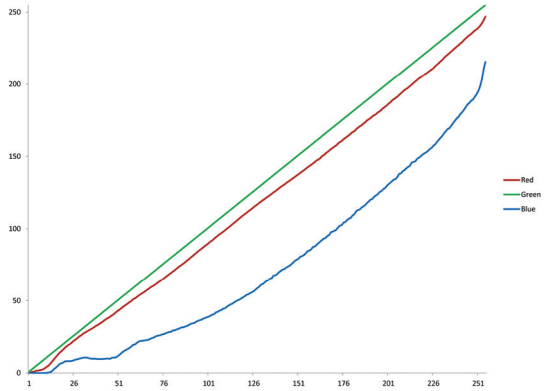

VIII
214 DAS

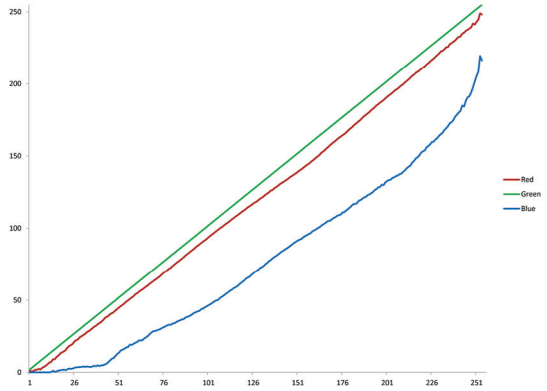

B

Days after sowing	*a*- coefficient of R equation	*a*- coefficient of B equation	*b*- coefficient of R equation	*b*- coefficient of B equation	R R^2	R *RMSE*	B R^2	B *RMSE*	GR NABC	GB NABC	RB NABC	%(GR/GB)
47	36.025	16.905	0.008	0.010	0.951	15.886	0.974	10.500	0.13	0.39	0.27	32.24
93	31.672	17.251	0.008	0.010	0.954	15.018	0.972	10.176	0.18	0.41	0.23	44.71
151	22.693	9.181	0.009	0.012	0.983	7.937	0.993	3.942	0.32	0.55	0.23	58.45
194	29.871	21.119	0.008	0.009	0.969	12.251	0.980	9.049	0.20	0.33	0.13	60.45
197	34.420	19.353	0.008	0.010	0.959	14.096	0.975	10.475	0.15	0.35	0.20	42.75
208	38.556	19.453	0.008	0.009	0.951	16.136	0.964	11.992	0.09	0.37	0.29	23.18
211	38.418	14.373	0.008	0.011	0.951	16.219	0.982	8.474	0.08	0.43	0.34	19.76
214	38.981	16.720	0.008	0.010	0.951	16.567	0.967	11.560	0.07	0.40	0.33	17.95
Mean	33.830	16.794	0.008	0.010	0.959	14.264	0.976	9.521	0.15	0.40	0.25	37.44
C.V.	0.17	0.22	0.06	0.07	0.01	0.21	0.01	0.27	0.54	0.17	0.28	0.45

The least values The highest values

C

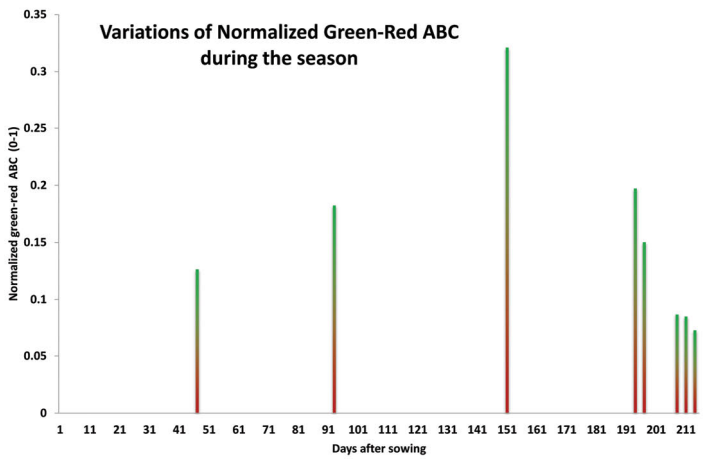

Fig. S5. Light attenuation trend in a ripening canopy, which is also compared with previous stages. (A) 255-tuple GSM is capable of detecting light interactions and attenuation even in a special kind of canopy, i.e. drying stand. Consider the shape of red curve which is approaching the green trend line. Obviously, only green pixels are included in 255-tuple GSM models. **(B)** Various growth stages are compared using exponential equations and curve characteristics. R, G, and B are red, green, and blue lights; NABC is the normalized area between curves, which is calculated by dividing each ABC value by the total area under the green line. **(C)** GR-NABC is proposed for determining the canopy growth stage.

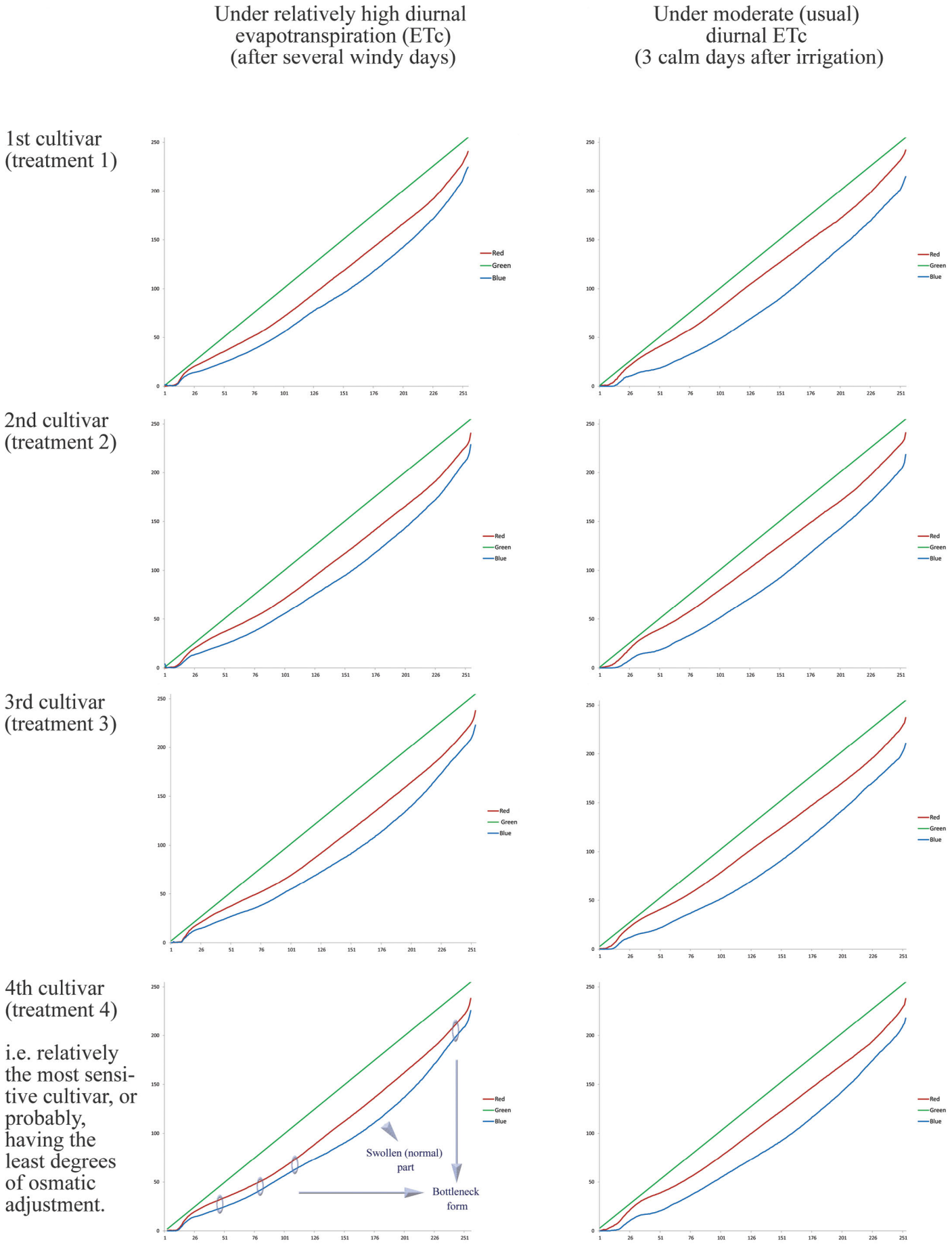

Fig. S6. Effect of water stress on light attenuation in canopies of 4 wheat cultivars. It seems that the overall result of variation in red and blue curves, results in a bottleneck and swollen forms, e.g. due to higher reflection of blue light in complete shadow.

1st cultivar (monoculture, treatment 1).

Physiological phase: spike emergence, (174 DAS).

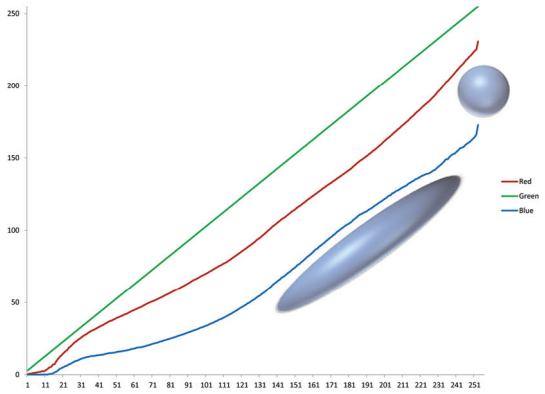

2nd cultivar (monoculture, treatment 2).

Physiological phase: spike emergence, (174 DAS).

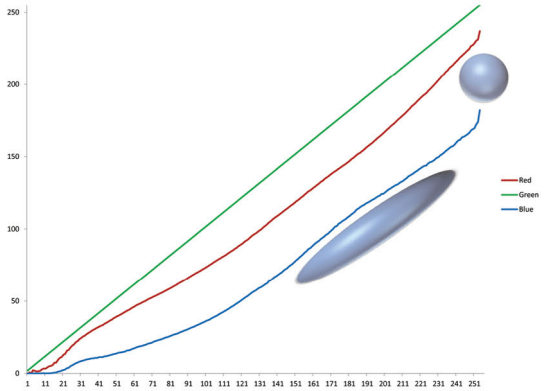

3rd cultivar (monoculture, treatment 3).

Physiological phase: late booting, (174 DAS).

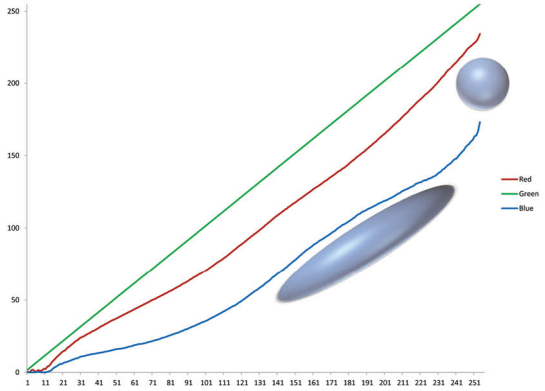

4th cultivar (monoculture, treatment 4).

Physiological phase: booting, (174 DAS).

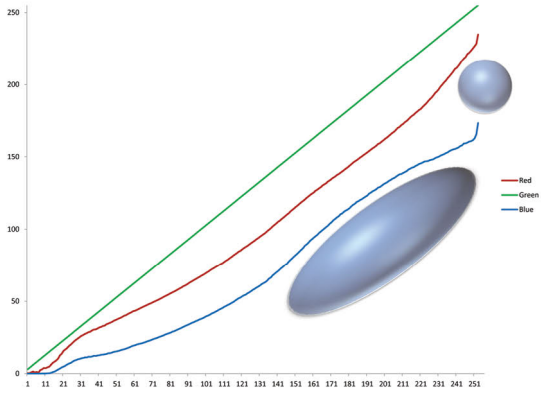

Fig. S7. Light attenuation trend in the canopy of 4 wheat cultivars, 4 days after a moderate cold stress. The most obvious impact was on the blue light trend, which has resulted in a deviation from the normal trend, due to an increase in the blue reflection (i.e. mainly less blue light absorption) in the range of B_{2-4} curve areas (green points either exposed to direct sunlight, or located in partial shade, see the manuscript). Moreover, compared to the curves of non-stress conditions, there is a considerable difference between the maximum values of red and blue (near 255, full sun light). The interferences of cold stress have been shown by ellipsoids and spheres of different sizes (i.e. related to different tolerances of the cultivars).

Fig. S8. General concepts and description of Double-Shot Light Balance Equations (DLBE). (A) Detailed description of the process in which the relative portion of absorbed light is calculated based on normalized values. **(B & C)** Mathematical demonstrations for the relationship between vertical and horizontal equations of normalized light values (see the tables providing general variables or mean values of the present experiment). **(D)** General mathematical light identities for DLBE.

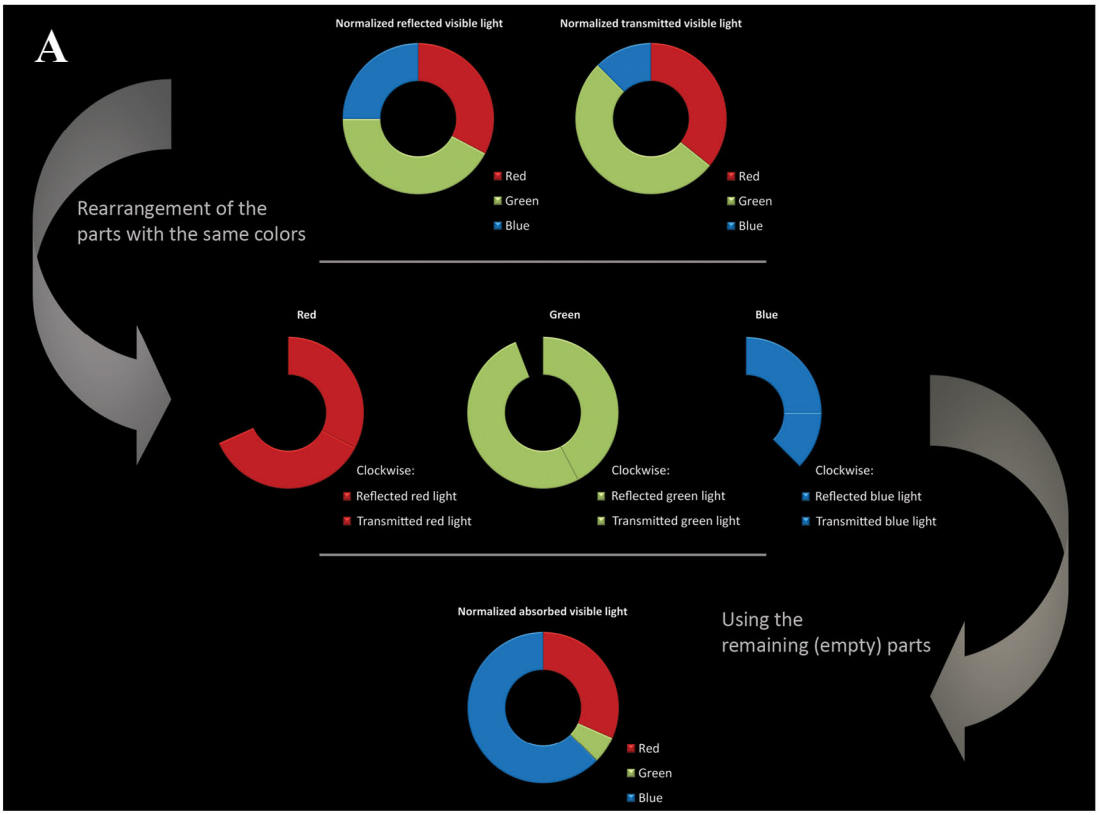

B

Mathematical proof for general form of DLBE

Based on definitions of normalized R, G, and B (see the manuscript and tables of the present figure), we have:

$$\begin{cases} NR_r = \dfrac{R_r}{R_r + G_r + B_r} \\ NG_r = \dfrac{G_r}{R_r + G_r + B_r} \\ NB_r = \dfrac{B_r}{R_r + G_r + B_r} \\ NR_{tr} = \dfrac{R_{tr}}{R_{tr} + G_{tr} + B_{tr}} \\ NG_{tr} = \dfrac{G_{tr}}{R_{tr} + G_{tr} + B_{tr}} \\ NB_{tr} = \dfrac{B_{tr}}{R_{tr} + G_{tr} + B_{tr}} \\ \textit{it is obvious that:} \\ NR_r + NG_r + NB_r = 1 \\ NR_{tr} + NG_{tr} + NB_{tr} = 1 \end{cases}$$

I. We want to show that if the summations of normalized reflected and transmitted components are subtracted from the related total received (input) light with an assumed value of 1, the summation of the resulted values will also be equal to 1. In other words, we want to show that:

$$(1 - NR_r - NR_{tr}) + (1 - NG_r - NG_{tr}) + (1 - NB_r - NB_{tr}) = 1$$

Let's spread the equation:

$$1 - \frac{R_r}{R_r + G_r + B_r} - \frac{R_{Tr}}{R_{tr} + G_{tr} + B_{tr}} + 1 - \frac{G_r}{R_r + G_r + B_r} - \frac{G_{tr}}{R_{tr} + G_{tr} + B_{tr}} + 1 - \frac{B_r}{R_r + G_r + B_r} - \frac{B_{tr}}{R_{tr} + G_{tr} + B_{tr}} = 1$$

Adding the ratios with similar denominators, the assumption will be proved:

$$3 - \left(\frac{R_r + G_r + B_r}{R_r + G_r + B_r} + \frac{R_{tr} + G_{tr} + B_{tr}}{R_{tr} + G_{tr} + B_{tr}}\right) = 1$$

i.e.:

1=1 ■

II. Alternatively, we may show that the total amount of T (as the result of adding the three components of normalized reflected, absorbed, and transmitted lights in a single band e.g. blue), will be equal to 1; or in other words, the normalized components (table cells) of horizontal equations may also been participated in the vertical equations without any conversion. We have:

$$\begin{cases} NR_r + NR_{tr} + NR_a = NG_r + NG_{tr} + NG_a = NB_r + NB_{tr} + NB_a = T \\ NR_r + NG_r + NB_r = 1 \\ NR_{tr} + NG_{tr} + NB_{tr} = 1 \\ NR_a + NG_a + NB_a = 1 \end{cases}$$

Using equations (1) and (4):

$$(T - NR_r - NR_{tr}) + (T - NG_r - NG_{tr}) + (T - NB_r - NB_{tr}) = 1$$

i.e.:

$$T - \frac{R_r}{R_r + G_r + B_r} - \frac{R_{Tr}}{R_{tr} + G_{tr} + B_{tr}} + T - \frac{G_r}{R_r + G_r + B_r} - \frac{G_{tr}}{R_{tr} + G_{tr} + B_{tr}} + T - \frac{B_r}{R_r + G_r + B_r} - \frac{B_{tr}}{R_{tr} + G_{tr} + B_{tr}} = 1$$

Adding the ratios with similar denominators, the assumption will be proved:

$$3T - \left(\frac{R_r + G_r + B_r}{R_r + G_r + B_r} + \frac{R_{tr} + G_{tr} + B_{tr}}{R_{tr} + G_{tr} + B_{tr}}\right) = 1$$

$$3T - 2 = 1$$

$$T = 1 \quad ■$$

C

Visible light	Normalized Red	Normalized Green	Normalized Blue	
Normalized total input visible light (255)	**1**	**1**	**1**	**Total**
Normalized total reflected visible light	Rr/(Rr+Gr+Br)	Gr/(Rr+Gr+Br)	Br/(Rr+Gr+Br)	**1**
Normalized total transmitted visible light	Rtr/(Rtr+Gtr+Btr)	Gtr/(Rtr+Gtr+Btr)	Btr/(Rtr+Gtr+Btr)	**1**
Normalized total absorbed visible light	Ra/(Ra+Ga+Ba)	Ga/(Ra+Ga+Ba)	Ba/(Ra+Ga+Ba)	**1**

R: Red, G: Green, B: Blue
r: reflected, tr: transmitted, a: absorbed
e.g.: Rr/(Rr+Gr+Br): Normalized Rreflected Red: NRr

Visible light	Red	Green	Blue	
Normalized total input visible light (255)	**1**	**1**	**1**	**Total**
Normalized total reflected visible light	0.33	0.42	0.25	**1**
Normalized total transmitted visible light	0.36	0.52	0.12	**1**
Normalized total absorbed visible light	0.32	0.06	0.63	**x=1**

R: Red, G: Green, B: Blue
r: reflected, tr: transmitted, a: absorbed; e.g.: Rr/(Rr+Gr+Br): Normalized Rreflected Red: NRr
Values are means over 15 treatments include mono- and mixed cropping of wheat cultivars, 6 replicates.

D

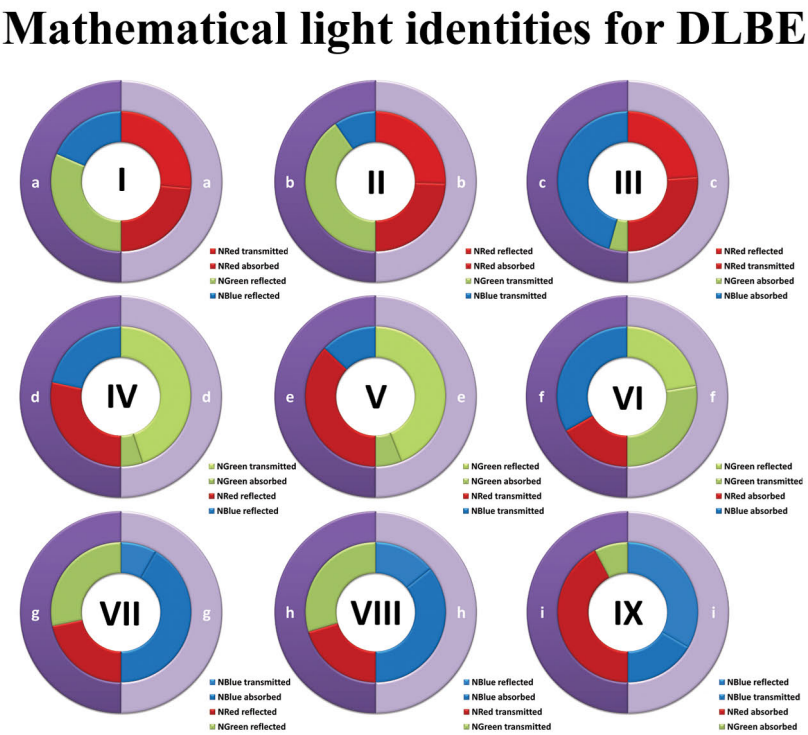

A

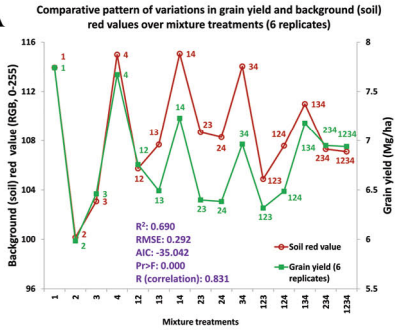

B

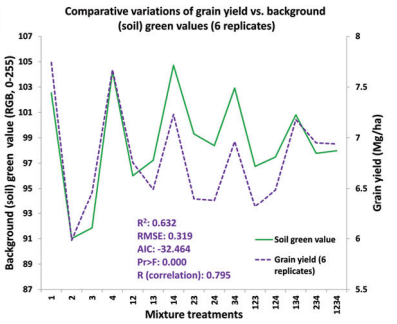

C

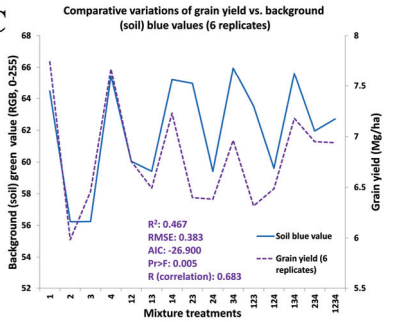

D

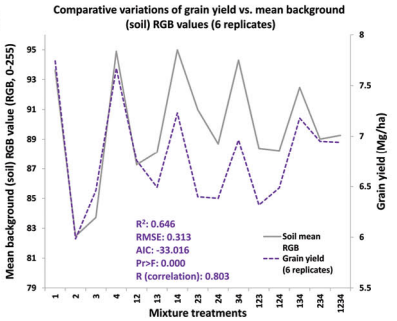

E

%Similarity between clustering of mixture treatments based on grain yield (with 6 replicates) and background (soil) color values

K-means clusters	Based on soil (bg*) red (%)	Based on soil (bg) green (%)	Based on soil (bg) blue (%)	Based on soil (bg) mean RGB (%)	Total mean (over the 4 color indices, %)
2	86.67	80.00	60.00	80.00	76.67
3	60.00	53.33	46.67	53.33	53.33
4	46.67	53.33	53.33	53.33	51.67
5	60.00	46.67	46.67	46.67	50.00
6	46.67	33.33	26.67	33.33	35.00
7	46.67	33.33	26.67	26.67	33.33
8	40.00	26.67	33.33	26.67	31.67
9	46.67	46.67	40.00	60.00	48.33
10	46.67	40.00	40.00	46.67	43.33
Mean	**53.33**	45.93	41.48	47.41	47.04

* bg: image (non vegetation) background; for full comparison, see the related supplemental data.

F

Total number of image pixels, averaged over 6 replicates/90 plots (8 megapixel): **7,990,272**

Canopy coverage (%vegetation): **% 83.75.**

Background (non vegetation) pixels: **1,298,020.889 (%16.25).**

G

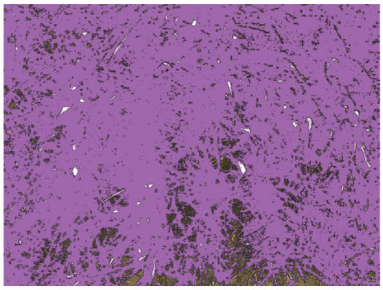

Background pixels including high reflective vegetation points (in which, green values are less than red, i.e. a non-vegetation reflectance behavior. see descriptions for segmentation type 1).

Non-masked area: **1,28,020.889 pixels (%16.25).**

H

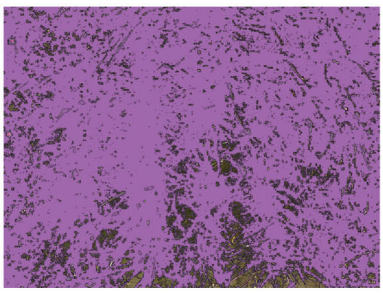

Absolute soil area, i.e. background excluding high reflective pixels.

Non-masked area: **1,231,736.378 pixels (%15.42)**

I

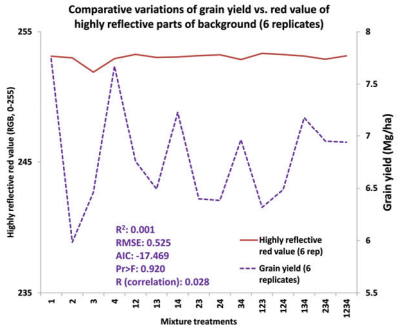

J

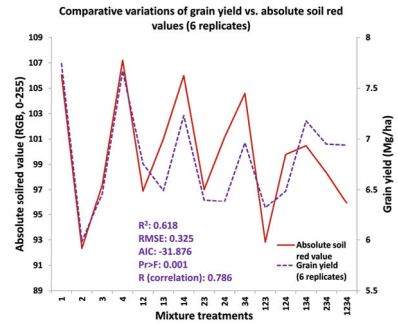

K

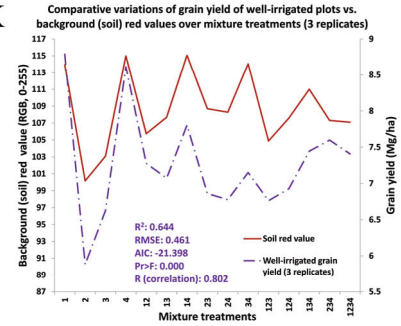

L

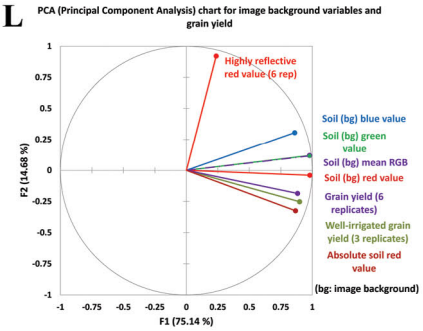

M

Comparison of (currently available and new) vegetation color indices for classification of canopies based on instant reflectance behavior, and grain yield prediction over various monocultures and mixtures (6 replicates).

Mixture treatments	%Canopy Coverage	G/R	G-R	NRI_{veg}	NGI_{veg}	NBI_{veg}	VI_{green}	$SAVI_{green}$	TGI	R_{soil}	G_{soil}	B_{soil}	Mean soil R,G,B	R_{veg}	G_{veg}	B_{veg}	$R_{veg}+R_{soil}$
1	82.42 a	1.36 ab	36.67 abc	0.332 a	0.450 abc	0.218 a	0.152 ab	0.227 ab	5611.26 a	113.94 a	102.54 a	64.47 a	93.65 a	103.03 a	139.70 a	67.57 a	216.97 a
2	86.02 a	1.35 ab	35.33 bcd	0.331 a	0.446 abc	0.222 a	0.148 ab	0.221 ab	5368.68 ab	100.16 a	91.02 a	56.23 a	82.47 a	101.87 a	137.20 a	68.32 a	202.03 a
3	80.81 a	1.31 b	32.35 d	0.334 a	0.437 d	0.229 a	0.133 b	0.200 b	5057.94 b	103.08 a	91.85 a	56.25 a	83.72 a	105.32 a	137.67 a	72.24 a	208.40 a
4	84.72 a	1.38 a	39.44 a	0.328 a	0.453 a	0.218 a	0.160 a	0.240 a	5828.91 a	114.99 a	104.24 a	65.45 a	94.89 a	103.57 a	143.01 a	68.87 a	218.57 a
12	85.84 a	1.37 a	37.26 abc	0.329 a	0.451 ab	0.219 a	0.156 a	0.234 a	5565.07 ab	105.74 a	96.01 a	60.04 a	87.26 a	100.92 a	138.18 a	67.17 a	206.66 a
13	81.22 a	1.33 ab	34.53 cd	0.334 a	0.444 bcd	0.222 a	0.141 ab	0.211 ab	5416.80 ab	107.68 a	97.22 a	59.41 a	88.10 a	105.85 a	140.38 a	70.24 a	213.53 a
14	84.23 a	1.37 ab	37.93 ab	0.330 a	0.450 abc	0.220 a	0.155 a	0.231 a	5672.26 a	115.06 a	104.71 a	65.20 a	94.99 a	103.98 a	141.91 a	69.50 a	219.05 a
23	85.06 a	1.34 ab	34.91 bcd	0.331 a	0.443 bcd	0.225 a	0.144 ab	0.216 ab	5316.56 ab	108.69 a	99.31 a	64.96 a	90.98 a	103.95 a	138.86 a	70.62 a	212.64 a
24	80.70 a	1.35 ab	36.28 abc	0.334 a	0.451 ab	0.215 a	0.148 ab	0.222 ab	5691.15 a	108.28 a	98.38 a	59.41 a	88.69 a	104.43 a	140.71 a	67.02 a	212.71 a
34	81.27 a	1.34 ab	35.38 bcd	0.331 a	0.444 bcd	0.225 a	0.145 ab	0.217 ab	5375.42 ab	114.04 a	102.92 a	65.95 a	94.30 a	104.37 a	139.75 a	70.81 a	218.41 a
123	84.88 a	1.34 ab	35.90 bc	0.329 a	0.442 cd	0.229 a	0.146 ab	0.219 ab	5330.14 ab	104.88 a	96.74 a	63.52 a	88.38 a	105.09 a	140.99 a	73.10 a	209.97 a
124	84.23 a	1.35 ab	36.54 abc	0.333 a	0.450 abc	0.217 a	0.150 ab	0.225 ab	5626.27 a	107.58 a	97.49 a	59.61 a	88.22 a	103.66 a	140.20 a	67.75 a	211.23 a
134	85.63 a	1.36 ab	36.59 abc	0.328 a	0.445 bcd	0.228 a	0.152 ab	0.227 ab	5358.31 ab	110.99 a	100.81 a	65.60 a	92.47 a	102.60 a	139.19 a	71.23 a	213.60 a
234	83.61 a	1.35 ab	36.32 abc	0.329 a	0.444 bcd	0.227 a	0.149 ab	0.223 ab	5396.71 ab	107.30 a	97.78 a	61.95 a	89.01 a	104.07 a	140.39 a	71.63 a	211.37 a
1234	85.67 a	1.36 ab	36.65 abc	0.329 a	0.447 abc	0.223 a	0.152 ab	0.227 ab	5474.62 ab	107.10 a	97.98 a	62.71 a	89.26 a	102.91 a	139.57 a	69.71 a	210.01 a
Mean	83.75	1.35	36.14	0.331	0.446	0.223	0.149	0.223	5472.67	108.63	98.60	62.05	89.76	103.71	139.85	69.72	212.34
P value	0.763	**0.011**	**0.000**	0.832	**0.000**	0.079	**0.010**	**0.010**	**0.001**	0.328	0.334	0.723	0.447	0.991	0.930	0.061	0.758
Criteria for linear relationship of color indices with grain yield (6 replicates)																	
R2	0.000	0.350	0.391	0.225	0.210	0.049	0.345	0.345	0.251	0.690	0.632	0.467	0.646	0.032	0.252	0.018	0.536
RMSE	0.525	0.424	0.410	0.462	0.467	0.512	0.425	0.425	0.455	0.292	0.319	0.383	0.313	0.517	0.454	0.521	0.358
AIC	-17.46	-23.92	-24.90	-21.29	-20.99	-18.21	-23.81	-23.81	-21.79	-35.04	-32.46	-26.90	-33.02	-17.94	-21.82	-17.73	-28.97
Model Pr>F	0.953	0.020	0.013	0.074	0.086	0.427	0.021	0.021	0.057	0.0001	0.0004	0.005	0.0003	0.526	0.056	0.631	0.002
R (correlation)	0.017	0.592	0.626	-0.475	0.458	-0.222	0.588	0.588	0.501	0.831	0.795	0.683	0.803	-0.178	0.502	-0.135	0.732

Mixture treatments are monocultures and mixtures of four early to middle ripening wheat cultivars in an RCB experimental design with six replicates. Each digit stands for a single cultivar, so the treatment 1234 shows the 4-component mixtures of cultivars 1,2,3 and 4. Values of each column with similar letters are not significantly different; Tukey, P<0.05. Color indices of Canopy coverage (%CC), VIgreen, SAVIgreen are taken from Li *et al* (2010) paper; G/R, G-R, NRIveg and NGIveg are taken from the paper of Wang *et al* (2013); and TGI is "triangular greenness index" (Hunt Jr., 2013). Rsoil, Gsoil, Rveg, Gveg, and Bveg are red, green, and blue values of soil (background) and vegetation, respectively. Mean soil RGB is also the averaged value of soil red, green and blue values.

Fig. S9. Various evaluations show the comparative advantage of background red value in resembling (predicting) relative patterns of wheat grain yield. (A-J) Comparative analyses of image background in relation to grain yield. **M.** Evaluation of image-derived indices available in literature for potential use in grain yield prediction, compared with our criteria.

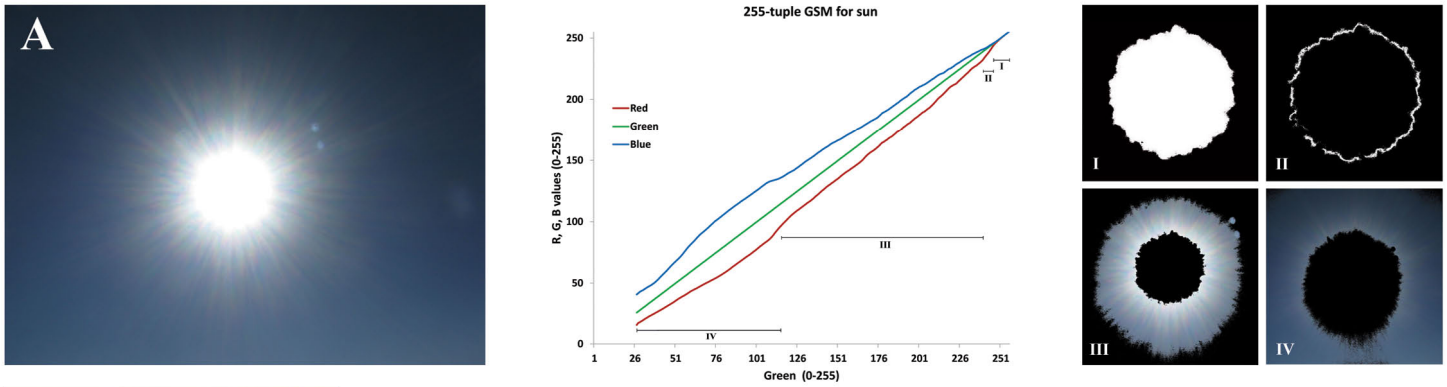

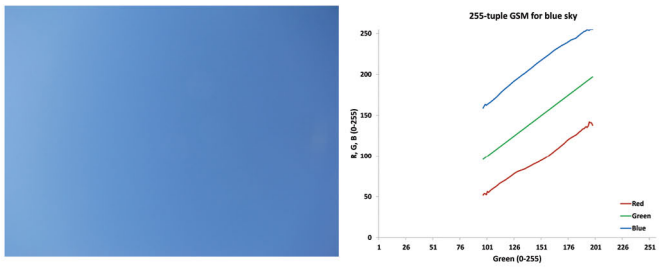

Fig. S10. 255-tuple GSM for "sun perspective" (as the source of light) and some other canopies. (A) Despite the green canopies, the red, green and blue trends in 255-tuple GSM of "sun perspective" are convergent at the highest intensities (i.e. the sun), and become divergent at the least intensities. The first diffraction of the three bands is recognizable where the red curve leaves the other two (part II as a ring around the sun). The 255-tuple GSM for blue sky lacks the complete light gradient. **(B)** The sample canopies of various species (either as a single plant or as a conventional canopy). The images are taken in autumn.

B

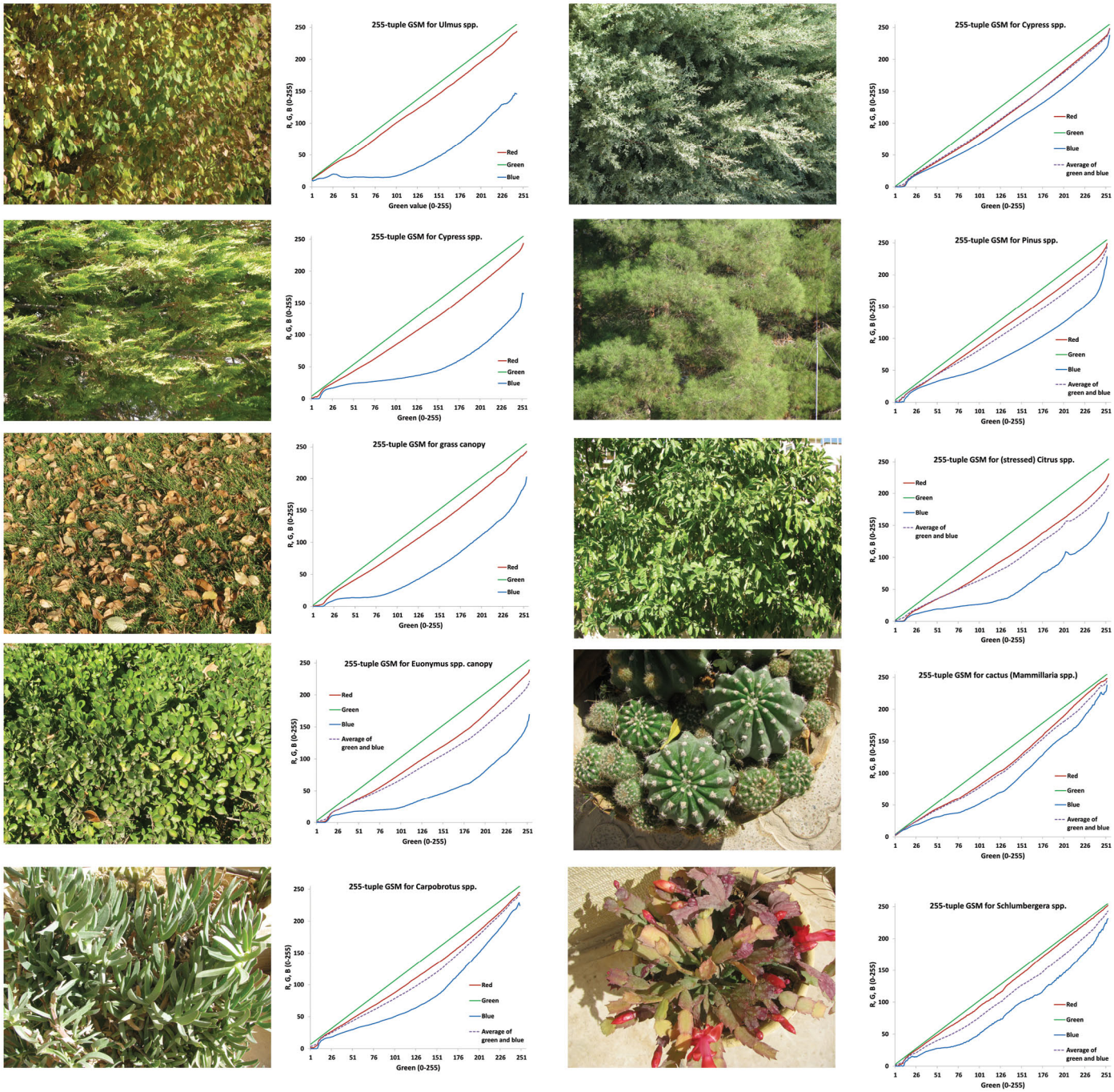

Table S1. Comparative evaluation for GSM equations based on fitness indices. Three monoculture samples (including cultivars 1, 3, and 4) were analyzed in 3- to 10- and 255-tuple GSMs.

Sample	Segmented parts	Fitness index	Red				Green				Blue			
			Linear	Polynomial	Exponential	Power	Linear	Polynomial	Exponential	Power	Linear	Polynomial	Exponential	Power
1	3	R^2	0.947	NA	0.999	0.981	0.986	NA	0.997	0.994	0.917	NA	0.999	0.987
	3	RMSE	22.475	NA	2.450	14.460	13.660	NA	6.515	9.023	26.626	NA	3.197	12.090
	3	AIC	-2.622	NA	-15.918	-5.268	-5.609	NA	-10.051	-8.097	-1.605	NA	-14.323	-6.342
	4	R^2	0.939	0.993	1.000	0.980	0.989	1.000	0.990	0.996	0.895	0.996	0.999	0.986
	4	RMSE	20.365	5.459	1.375	12.792	10.205	1.471	9.931	6.150	25.424	7.078	2.194	11.109
	4	AIC	NA	-23.967	NA	NA	NA	-34.454	NA	NA	NA	-21.889	NA	NA
	5	R^2	0.943	0.997	0.999	0.982	0.993	1.000	0.983	0.998	0.891	0.993	0.999	0.985
	5	RMSE	18.010	5.259	2.373	11.170	7.705	1.892	12.319	4.259	23.567	7.342	2.167	10.408
	5	AIC	56.355	NA	36.087	51.578	47.864	NA	52.557	41.937	59.044	NA	35.181	50.872
	6	R^2	0.946	0.996	0.998	0.983	0.994	1.000	0.978	0.998	0.889	0.990	0.998	0.983
	6	RMSE	16.588	5.359	3.263	10.321	6.583	2.016	13.206	3.566	22.247	7.608	2.677	10.120
	6	AIC	49.272	63.986	29.760	43.577	38.180	52.252	46.535	30.823	52.794	68.191	27.383	43.341
	7	R^2	0.951	0.996	0.997	0.984	0.996	1.000	0.973	0.999	0.892	0.989	0.998	0.983
	7	RMSE	15.258	5.086	4.073	9.433	5.381	1.938	14.243	2.774	20.994	7.373	2.923	9.651
	7	AIC	49.796	46.853	31.306	43.064	35.205	33.346	48.833	25.931	54.264	52.053	26.661	43.384
	8	R^2	0.958	0.997	0.995	0.987	0.998	1.000	0.967	1.000	0.901	0.991	0.998	0.985
	8	RMSE	13.983	4.301	4.844	8.396	3.971	1.471	15.488	1.720	19.911	6.528	2.719	8.873
	8	AIC	51.904	40.914	34.942	43.743	31.764	23.751	53.540	18.372	57.559	47.591	25.705	44.626
	9	R^2	0.958	0.995	0.994	0.986	0.998	1.000	0.966	0.999	0.898	0.989	0.997	0.983
	9	RMSE	13.563	4.862	5.202	8.435	3.846	1.627	15.401	1.876	19.350	7.001	3.364	9.101
	9	AIC	55.470	42.816	38.222	46.921	32.785	23.108	57.758	19.862	61.867	49.380	30.377	48.289
	10	R^2	0.958	0.995	0.993	0.986	0.998	1.000	0.965	0.999	0.897	0.987	0.996	0.981
	10	RMSE	13.169	5.076	5.490	8.369	3.651	1.673	15.441	1.899	18.855	7.122	3.684	9.131
	10	AIC	59.325	44.926	41.828	50.258	33.668	22.731	62.509	20.598	66.504	51.697	33.847	52.002
	255	R^2	0.977	0.996	0.982	0.991	NA	NA	NA	NA	0.927	0.992	0.994	0.987
	255	RMSE	8.873	3.760	8.119	5.974	NA	NA	NA	NA	14.263	4.798	4.319	6.668
	255	AIC	1106.582	677.827	911.972	NA	NA	NA	NA	NA	1346.756	801.672	747.187	967.822
2	3	R^2	0.954	NA	1.000	0.981	0.988	NA	0.996	0.995	0.923	NA	1.000	0.990
	3	RMSE	20.879	NA	1.652	13.989	12.246	NA	7.298	7.985	26.637	NA	1.861	11.004
	3	AIC	-3.063	NA	-18.283	-5.466	-6.264	NA	-9.370	-8.831	-1.602	NA	-17.569	-6.906
	4	R^2	0.953	0.999	1.000	0.983	0.992	1.000	0.988	0.998	0.912	0.999	1.000	0.992
	4	RMSE	17.781	2.908	1.123	11.451	8.675	0.154	10.796	5.001	23.858	2.994	1.649	8.783
	4	AIC	NA	-29.005	NA	NA	NA	-52.536	NA	NA	NA	-28.772	NA	NA
	5	R^2	0.961	1.000	0.998	0.988	0.995	1.000	0.978	0.999	0.915	0.999	0.999	0.993
	5	RMSE	14.972	2.050	3.482	9.193	6.058	1.940	13.526	3.033	21.413	2.429	2.680	7.355
	5	AIC	54.508	NA	39.922	49.631	45.460	NA	53.492	38.541	58.086	NA	37.305	47.400
	6	R^2	0.963	0.999	0.997	0.989	0.996	1.000	0.974	0.999	0.914	0.999	0.999	0.993
	6	RMSE	13.788	2.373	4.243	8.387	5.151	1.598	14.123	2.415	20.299	2.945	2.776	6.939
	6	AIC	47.053	54.213	32.912	41.088	35.238	49.469	47.341	26.149	51.694	56.803	27.818	38.813
	7	R^2	0.967	0.999	0.995	0.990	0.997	1.000	0.969	1.000	0.918	0.998	0.998	0.994
	7	RMSE	12.608	2.402	5.243	7.506	4.179	1.708	15.038	1.860	19.162	2.966	3.425	6.349
	7	AIC	47.125	36.350	34.840	34.840	31.665	31.581	49.593	20.335	52.986	39.304	28.881	37.522
	8	R^2	0.972	0.999	0.992	0.993	0.998	1.000	0.963	1.000	0.925	0.999	0.996	0.995
	8	RMSE	11.566	1.932	6.462	6.550	3.218	1.921	16.301	1.529	18.281	2.181	4.451	5.511
	8	AIC	48.868	28.107	39.554	39.771	28.398	28.023	54.358	16.494	56.192	30.048	33.589	37.007
	9	R^2	0.972	0.999	0.991	0.992	0.999	1.000	0.962	1.000	0.923	0.998	0.996	0.995
	9	RMSE	11.164	2.638	6.581	6.490	2.874	1.399	16.133	1.109	17.846	2.956	4.137	5.689
	9	AIC	51.966	31.811	42.455	42.203	27.539	20.389	58.594	10.407	60.410	33.860	34.099	39.831
	10	R^2	0.972	0.998	0.990	0.992	0.999	1.000	0.961	1.000	0.921	0.998	0.996	0.994
	10	RMSE	10.903	3.066	6.727	6.512	2.634	1.068	16.047	0.880	17.549	3.292	4.036	5.803
	10	AIC	55.550	34.843	45.890	45.243	27.140	13.746	63.278	5.223	65.069	36.262	35.672	42.936
	255	R^2	0.980	0.996	0.981	0.991	NA	NA	NA	NA	0.932	0.996	0.992	0.994
	255	RMSE	8.795	3.835	8.949	6.023	NA	NA	NA	NA	15.279	3.629	5.485	5.303
	255	AIC	1102.106	687.777	916.171	NA	NA	NA	NA	NA	1381.581	659.781	868.619	851.507
3	3	R^2	0.940	NA	0.998	0.972	0.983	NA	0.999	0.991	0.909	NA	0.999	0.987
	3	RMSE	23.064	NA	4.597	16.484	14.946	NA	4.154	11.254	27.295	NA	3.620	11.948
	3	AIC	-2.466	NA	-12.144	-4.481	-5.069	NA	-12.751	-6.771	-1.456	NA	-13.577	-6.412
	4	R^2	0.933	0.998	0.999	0.973	0.988	1.000	0.992	0.995	0.890	0.996	1.000	0.988
	4	RMSE	20.740	5.552	2.285	14.161	10.623	1.049	9.031	7.011	25.718	6.511	1.837	10.250
	4	AIC	NA	-23.831	NA	NA	NA	-37.165	NA	NA	NA	-22.557	NA	NA
	5	R^2	0.938	0.996	0.999	0.976	0.992	1.000	0.984	0.997	0.883	0.993	0.999	0.987
	5	RMSE	18.461	6.042	2.383	12.457	7.954	1.660	11.611	4.836	24.171	7.218	1.757	9.714
	5	AIC	56.602	NA	36.130	52.668	48.183	NA	51.966	43.206	59.297	NA	33.082	50.181
	6	R^2	0.940	0.994	0.998	0.977	0.994	1.000	0.980	0.998	0.879	0.989	0.998	0.984
	6	RMSE	17.061	6.467	3.371	11.574	6.829	1.856	12.563	4.066	23.087	8.068	2.804	9.753
	6	AIC	49.609	66.242	30.149	44.952	38.621	51.264	45.936	32.398	53.238	68.896	27.938	42.899
	7	R^2	0.946	0.993	0.996	0.979	0.995	1.000	0.975	0.999	0.881	0.986	0.996	0.982
	7	RMSE	15.746	6.396	4.191	10.673	5.650	1.833	13.663	3.211	21.993	8.471	3.789	9.699
	7	AIC	50.237	50.062	31.707	44.792	35.889	32.566	48.250	27.977	54.915	53.996	30.295	43.453
	8	R^2	0.953	0.994	0.995	0.982	0.997	1.000	0.969	0.999	0.888	0.985	0.995	0.982
	8	RMSE	14.460	5.880	4.923	9.627	4.191	1.332	15.015	2.029	21.055	8.376	4.344	9.406
	8	AIC	52.440	45.917	35.200	45.931	32.626	22.155	53.043	21.019	58.453	51.579	33.201	45.560
	9	R^2	0.954	0.991	0.992	0.981	0.998	1.000	0.968	0.999	0.887	0.981	0.993	0.979
	9	RMSE	13.864	6.538	5.820	9.498	4.019	1.597	15.054	2.111	20.298	8.888	5.141	9.616
	9	AIC	55.866	48.149	40.243	49.057	33.575	22.782	57.348	21.984	62.728	53.675	38.010	49.280
	10	R^2	0.956	0.990	0.990	0.980	0.998	1.000	0.966	0.999	0.887	0.979	0.991	0.977
	10	RMSE	13.348	6.877	6.489	9.348	3.781	1.690	15.191	2.085	19.675	9.088	5.619	9.683
	10	AIC	59.596	50.996	45.172	52.472	34.368	22.930	62.182	22.467	67.356	56.572	42.290	53.176
	255	R^2	0.976	0.993	0.980	0.988	NA	NA	NA	NA	0.919	0.986	0.990	0.984
	255	RMSE	8.926	4.848	8.458	6.646	NA	NA	NA	NA	14.854	6.099	5.320	7.113
	255	AIC	1109.598	806.890	NA	966.139	NA	NA	NA	NA	1367.331	923.475	853.080	1000.646
Mean	3	R^2	0.947	NA	0.999	0.978	0.986	NA	0.997	0.993	0.916	NA	0.999	0.988
	3	RMSE	22.139	NA	2.900	14.978	13.617	NA	5.989	9.420	26.853	NA	2.893	11.681
	3	AIC	-2.717	NA	-15.448	-5.072	-5.648	NA	-10.724	-7.900	-1.554	NA	-15.156	-6.553
	4	R^2	0.942	0.997	1.000	0.979	0.990	1.000	0.990	0.996	0.899	0.997	0.999	0.988
	4	RMSE	19.628	4.640	1.594	12.801	9.834	0.891	9.920	6.054	25.000	5.528	1.893	10.047
	4	AIC	NA	-25.601	NA	NA	NA	-41.385	NA	NA	NA	NA	NA	NA
	5	R^2	0.947	0.997	0.999	0.982	0.993	1.000	0.982	0.998	0.897	0.995	0.999	0.988
	5	RMSE	17.148	4.451	2.746	10.940	7.239	1.831	12.485	4.043	23.050	5.663	2.202	9.159
	5	AIC	55.822	NA	37.380	51.292	47.169	NA	52.672	41.228	58.809	NA	35.189	49.484
	6	R^2	0.950	0.996	0.997	0.983	0.995	1.000	0.977	0.999	0.894	0.993	0.998	0.987
	6	RMSE	15.812	4.733	3.626	10.094	6.187	1.823	13.297	3.349	21.877	6.207	2.752	8.937
	6	AIC	48.644	61.480	30.940	43.206	37.346	50.995	46.604	29.790	52.575	64.630	27.713	41.684
	7	R^2	0.954	0.996	0.996	0.984	0.996	1.000	0.972	0.999	0.897	0.991	0.997	0.986
	7	RMSE	14.537	4.628	4.502	9.204	5.070	1.826	14.315	2.615	20.717	6.270	3.379	8.567
	7	AIC	49.053	44.422	32.618	40.899	34.253	32.498	48.892	24.748	54.055	48.451	28.612	41.453
	8	R^2	0.961	0.997	0.994	0.987	0.998	1.000	0.967	1.000	0.904	0.992	0.996	0.988
	8	RMSE	13.336	4.037	5.410	8.191	3.793	1.575	15.601	1.759	19.749	5.695	3.838	7.930
	8	AIC	51.071	38.313	36.565	43.149	30.929	24.643	53.647	18.629	57.401	43.073	30.832	42.398
	9	R^2	0.961	0.995	0.992	0.986	0.998	1.000	0.965	1.000	0.902	0.989	0.995	0.985
	9	RMSE	12.863	4.679	5.868	8.141	3.579	1.541	15.530	1.699	19.165	6.282	4.214	8.135
	9	AIC	54.434	40.925	40.307	46.060	31.300	22.093	57.900	17.418	61.668	45.638	34.162	45.800
	10	R^2	0.962	0.994	0.991	0.986	0.998	1.000	0.964	1.000	0.902	0.988	0.994	0.984
	10	RMSE	12.473	5.007	6.235	8.076	3.355	1.477	15.559	1.622	18.693	6.501	4.446	8.206
	10	AIC	58.157	43.588	44.297	49.324	31.725	19.802	62.656	16.096	66.310	48.177	37.270	49.371
	255	R^2	0.978	0.995	0.981	0.990	NA	NA	NA	NA	0.926	0.991	0.992	0.988
	255	RMSE	8.864	4.148	8.509	6.214	NA	NA	NA	NA	14.799	4.842	5.041	6.361
	255	AIC	1106.096	724.164	914.071	966.139	NA	NA	NA	NA	1365.222	794.976	822.962	939.991

Table S2. Curve characteristics (equation indices) of 255–tuple GSM. For more information, please see Figure S3 and Materials and Method section.

Treatments	*a* coefficient of R equation	*a* coefficient of B equation	*b* coefficient of R equation	*b* coefficient of B equation	R R^2	R *RMSE*	B R^2	B *RMSE*	R Q_1	R Q_2	R Q_3	B Q_1	B Q_2	B Q_3	R Q_1-B Q_1	R Q_2-B Q_2	R Q_3-B Q_3	B Q_1/R Q_1	B Q_2/R Q_2	B Q_3/R Q_3
1	28.193 a	10.802 a	0.0082 a	0.0113 a	0.977 a	9.20 a	0.995 a	3.743 a	47.612 a	80.422 ab	135.867 bc	22.238 a	45.797 ab	94.352 b	25.374 a	34.625 a	41.515 a	0.469 a	0.571 a	0.695 a
2	28.394 a	11.252 a	0.0082 a	0.0113 a	0.979 a	8.86 a	0.995 a	3.807 a	47.960 a	81.026 ab	136.916 abc	23.124 a	47.537 ab	97.757 ab	24.837 a	33.489 a	39.158 a	0.484 a	0.588 a	0.714 a
3	29.151 a	11.778 a	0.0082 a	0.0114 a	0.976 a	9.86 a	0.994 a	4.552 a	49.350 a	83.550 a	141.464 a	24.360 a	50.391 a	104.257 a	24.989 a	33.159 a	37.207 a	0.495 a	0.604 a	0.737 a
4	27.296 a	10.201 a	0.0083 a	0.0115 a	0.978 a	8.82 a	0.992 a	4.550 a	46.255 a	78.396 b	132.894 c	21.259 a	44.314 b	92.388 b	24.996 a	34.082 a	40.506 a	0.461 a	0.566 a	0.696 a
12	27.440 a	10.751 a	0.0083 a	0.0113 a	0.979 a	8.70 a	0.994 a	3.871 a	46.560 a	79.022 ab	134.147 bc	22.137 a	45.593 ab	93.930 b	24.424 a	33.429 a	40.216 a	0.478 a	0.578 a	0.701 a
13	28.919 a	11.201 a	0.0082 a	0.0113 a	0.974 a	9.99 a	0.994 a	4.328 a	48.795 a	82.348 ab	138.998 ab	23.120 a	47.726 ab	98.527 ab	25.676 a	34.622 a	40.471 a	0.475 a	0.580 a	0.709 a
14	27.969 a	10.949 a	0.0082 a	0.0112 a	0.979 a	8.68 a	0.994 a	3.969 a	47.221 a	79.740 ab	134.679 bc	22.433 a	45.970 ab	94.227 b	24.788 a	33.770 a	40.452 a	0.477 a	0.578 a	0.700 a
23	28.339 a	11.567 a	0.0082 a	0.0112 a	0.976 a	9.58 a	0.994 a	4.405 a	47.949 a	81.143 ab	137.343 abc	23.601 a	48.163 ab	98.305 ab	24.348 a	32.980 a	39.039 a	0.494 a	0.594 a	0.716 a
24	28.942 a	10.601 a	0.0081 a	0.0113 a	0.975 a	9.47 a	0.993 a	4.084 a	48.452 a	81.122 ab	135.832 bc	21.798 a	44.832 b	92.230 b	26.654 a	36.290 a	43.602 a	0.450 a	0.553 a	0.679 a
34	28.187 a	11.225 a	0.0083 a	0.0113 a	0.976 a	9.53 a	0.994 a	4.207 a	47.782 a	81.006 ab	137.347 abc	23.136 a	47.697 ab	98.345 ab	24.645 a	33.309 a	39.002 a	0.485 a	0.590 a	0.716 a
123	28.357 a	12.021 a	0.0082 a	0.0111 a	0.976 a	9.42 a	0.993 a	4.491 a	47.893 a	80.913 ab	136.737 abc	24.383 a	49.467 ab	100.376 ab	23.511 a	31.446 a	36.361 a	0.511 a	0.612 a	0.734 a
124	28.196 a	10.581 a	0.0082 a	0.0113 a	0.976 a	9.38 a	0.994 a	4.094 a	47.578 a	80.292 ab	135.516 bc	21.851 a	45.129 b	93.213 b	25.727 a	35.163 a	42.303 a	0.460 a	0.563 a	0.688 a
134	27.302 a	11.513 a	0.0084 a	0.0112 a	0.979 a	8.95 a	0.994 a	4.088 a	46.611 a	79.591 ab	135.935 bc	23.598 a	48.385 ab	99.239 ab	23.012 a	31.206 a	36.696 a	0.509 a	0.609 a	0.730 a
234	28.099 a	11.656 a	0.0082 a	0.0111 a	0.978 a	9.09 a	0.994 a	4.230 a	47.548 a	80.474 ab	136.225 bc	23.754 a	48.423 ab	98.745 ab	23.794 a	32.051 a	37.481 a	0.500 a	0.602 a	0.725 a
1234	27.624 a	11.087 a	0.0083 a	0.0113 a	0.979 a	8.77 a	0.995 a	3.807 a	46.995 a	79.965 ab	136.089 bc	22.862 a	47.160 ab	97.327 ab	24.134 a	32.805 a	38.762 a	0.489 a	0.591 a	0.716 a
Mean	28.161	11.146	0.0082	0.0113	0.977	9.219	0.994	4.148	47.637	80.601	136.399	22.910	47.106	96.881	24.727	33.495	39.518	0.482	0.585	0.710
P value	0.721	0.078	0.896	0.569	0.503	0.141	0.089	0.091	0.481	0.093	**0.000**	**0.023**	**0.002**	**0.000**	0.939	0.883	0.581	0.719	0.547	0.201

Treatments are monocultures and mixtures of the four early to middle ripening wheat cultivars in an RCBD experimental design with six replicates. Each digit stands for a single cultivar, so the treatment 1234 shows the 4-component mixtures of cultivars 1,2,3 and 4. For definitions of indices, please see the Extended Data Fig. 1 and 3, and also the Methods section. Values of each column with similar letters are not significantly different; Tukey, P<0.05.

Table S3. Curve characteristics (primary area indices) of 255–tuple GSM. For more information, please see Figure S3 and Materials and Method section.

Treatments	R AUC	B AUC	GR ABC	GB ABC	RB ABC	GR_{01} ABC	GR_{12} ABC	GR_{23} ABC	GR_{34} ABC	GR_{45} ABC	GB_{01} ABC	GB_{12} ABC	GB_{23} ABC	GB_{34} ABC	GB_{45} ABC	R_{01} AUC	R_{12} AUC	R_{23} AUC	R_{34} AUC	R_{45} AUC	B_{01} AUC	B_{12} AUC	B_{23} AUC	B_{34} AUC	B_{45} AUC
1	23991.48 abc	15894.26 b	8517.77 abc	16614.99 a	8097.22 a	125.36 a	4061.71 abc	2960.58 a	1241.27 a	128.84 b	93.24 a	9182.11 a	4730.39 a	2367.77 a	241.47 a	178.97 a	9387.96 a	8484.75 a	5098.56 a	841.24 b	22.18 a	5605.14 a	5086.69 a	4368.14 a	812.11 b
2	24145.56 abc	16452.13 ab	8356.19 abc	16049.62 ab	7693.43 a	130.62 a	3914.25 abc	2876.11 a	1239.54 a	195.66 ab	88.31 a	8184.76 ab	4904.56 a	2497.04 a	374.94 a	177.29 a	9373.33 a	8136.72 a	5142.54 a	1278.42 ab	11.86 a	5052.49 ab	5430.85 a	4655.21 a	1267.77 ab
3	24962.40 a	17473.75 a	7548.10 c	15036.75 b	7488.65 a	102.57 a	3383.00 c	2615.75 a	1172.73 a	274.05 a	86.44 a	6091.23 b	5576.29 a	2804.22 a	478.57 a	107.18 a	8893.50 a	8460.67 a	5438.93 a	2062.12 a	13.31 a	3483.69 b	6161.96 a	5916.28 a	1898.51 a
4	23432.88 c	15551.31 b	9074.62 a	16956.19 a	7881.57 a	143.15 a	4828.78 a	2458.27 a	1422.69 a	221.71 ab	113.69 a	9311.86 a	4645.74 a	2461.83 a	423.07 a	157.01 a	10466.30 a	6465.64 a	5012.72 a	1331.20 ab	12.14 a	5517.64 a	4569.67 a	4074.51 a	1377.35 ab
12	23660.89 bc	15834.16 b	8847.20 ab	16673.93 a	7826.73 a	107.63 a	4432.38 ab	2886.75 a	1286.65 a	133.79 b	87.70 a	9005.90 a	4740.16 a	2610.20 a	229.96 a	123.29 a	9672.29 a	7949.41 a	5038.02 a	877.88 b	14.13 a	5401.52 a	5014.92 a	4621.88 a	781.71 b
13	24537.73 ab	16520.49 ab	7972.60 bc	15989.85 ab	8017.24 a	142.18 a	3668.64 bc	2952.93 a	1021.22 a	187.63 ab	113.83 a	7731.14 ab	5306.71 a	2505.17 a	332.99 a	165.24 a	9243.86 a	9219.16 a	4629.19 a	1242.75 b	12.83 a	4534.94 ab	5913.13 a	4924.66 a	1101.40 ab
14	23772.86 bc	15916.27 b	8733.47 ab	16590.06 a	7856.59 a	95.24 a	4387.97 abc	2885.71 a	1193.79 a	170.76 ab	86.32 a	9395.07 a	3854.05 a	2845.06 a	409.56 a	144.76 a	9853.70 a	8075.37 a	4698.46 a	1090.57 b	19.76 a	5901.43 a	3984.11 a	4793.27 a	1217.69 ab
23	24217.91 abc	16539.54 ab	8291.01 abc	15969.38 ab	7678.37 a	148.91 a	4010.43 abc	2851.01 a	1114.88 a	165.78 ab	116.03 a	8002.65 ab	5463.58 a	2073.19 a	313.92 a	184.67 a	9601.40 a	8444.99 a	4852.03 a	1097.62 b	13.80 a	4975.69 ab	6291.67 a	4146.81 a	1078.24 ab
24	24046.86 abc	15549.11 b	8460.39 abc	16958.14 a	8497.76 a	134.75 a	4146.87 abc	2760.92 a	1251.26 a	166.59 ab	114.10 a	9804.84 a	3795.18 a	2909.02 a	335.00 a	167.50 a	10073.04 a	7913.00 a	4840.32 a	1053.00 b	12.82 a	5981.41 a	3773.48 a	4730.31 a	1051.08 ab
34	24210.17 abc	16542.04 ab	8298.66 abc	15966.80 ab	7668.14 a	142.04 a	4030.38 abc	2770.91 a	1144.81 a	210.53 ab	110.38 a	8306.16 ab	4606.58 a	2539.16 a	404.52 a	131.55 a	9589.37 a	8209.76 a	4855.94 a	1423.56 ab	7.87 a	5218.34 ab	5074.25 a	4885.09 a	1436.48 ab
123	24153.33 abc	16896.92 ab	8356.59 abc	15612.99 ab	7256.40 a	161.05 a	3910.82 abc	3030.29 a	1069.02 a	185.41 ab	109.57 a	7814.86 ab	4984.91 a	2397.31 a	306.35 a	251.70 a	9385.09 a	8705.21 a	4569.23 a	1204.28 b	11.43 a	5038.06 ab	5909.43 a	4816.86 a	1087.02 ab
124	23935.46 abc	15705.10 b	8573.79 abc	16804.15 a	8230.36 a	158.38 a	4220.78 abc	2886.98 a	1137.54 a	170.11 ab	116.26 a	9362.75 a	4677.30 a	2343.74 a	304.10 a	206.29 a	9838.22 a	8226.44 a	4572.62 a	1091.89 b	23.08 a	5671.66 a	4969.20 a	4042.01 a	999.15 b
134	23927.48 abc	16712.33 ab	8582.61 abc	15797.75 ab	7215.14 a	96.51 a	4036.37 abc	3068.42 a	1132.22 a	249.10 ab	85.22 a	8287.69 ab	4414.43 a	2633.11 a	377.30 a	80.74 a	8959.38 a	8559.50 a	4695.70 a	1632.15 ab	10.28 a	5305.31 a	4985.24 a	5076.06 a	1335.45 ab
234	24033.81 abc	16630.91 ab	8474.44 abc	15877.34 ab	7402.90 a	142.14 a	4177.03 abc	2760.19 a	1174.56 a	220.52 ab	122.53 a	8030.41 ab	4819.97 a	2498.21 a	406.23 a	198.20 a	9758.63 a	7846.56 a	4775.27 a	1455.14 ab	20.89 a	5099.84 ab	5353.28 a	4722.79 a	1434.10 ab
1234	23963.02 abc	16382.77 ab	8543.39 abc	16123.64 ab	7580.25 a	119.80 a	4258.11 abc	2800.16 a	1140.04 a	225.28 ab	110.81 a	8172.70 ab	4773.46 a	2695.67 a	371.00 a	130.03 a	9663.05 a	8018.67 a	4660.46 a	1490.81 ab	16.94 a	5010.71 ab	5064.71 a	5030.33 a	1260.08 ab
Mean	24066.12	16306.74	8442.05	16201.44	7759.38	130.02	4097.84	2837.67	1182.82	193.72	103.63	8445.61	4752.89	2545.38	353.93	160.29	9583.94	8181.06	4852.67	1278.18	14.89	5186.52	5172.17	4714.95	1209.21
P value	**0.002**	**0.000**	**0.002**	**0.000**	0.769	0.199	**0.003**	0.910	0.908	**0.000**	0.287	**0.000**	0.509	0.790	0.417	0.456	0.812	0.579	0.988	**0.000**	0.235	**0.002**	0.101	0.338	**0.009**

Treatments are monocultures and mixtures of the four early to middle ripening wheat cultivars in an RCBD experimental design with six replicates. Each digit stands for a single cultivar, so the treatment 1234 shows the 4-component mixtures of cultivars 1,2,3 and 4. R AUC, B AUC, GR ABC, GB ABC, and RB ABC are the area under the red curve, the area under the blue curve, the area between green and red curves, the area between green and blue curves, and between red and blue curves, respectively. 01, 12, 23, 34, 45 subscripts of color curves (e.g. GR_{01}) indicate the curve regions of 01, 12, etc. Values of each column with similar letters are not significantly different; Tukey, P<0.05.

Table S4. Curve characteristics (secondary area indices) of 255−tuple GSM. For more information, please see Figure S3 and Materials and Method section.

Treatments	R_{02}/R_{04} AUC		B_{02}/B_{04} AUC		R_{01}-B_{01} AUC		R_{12}-B_{12} AUC		R_{23}-B_{23} AUC		R_{34}-B_{34} AUC		R_{45}-B_{45} AUC		GR_{01}/GB_{01} ABC		GR_{12}/GB_{12} ABC		GR_{23}/GB_{23} ABC		GR_{34}/GB_{34} ABC		GR_{45}/GB_{45} ABC		Total GR/GB ABC		(R to B ratio$_{34}$)/(R to	
1	0.41	a	0.37	a	156.79	a	3782.82	a	3398.06	a	730.42	a	29.13	a	1.42	a	0.45	a	0.64	a	0.53	a	0.55	a	0.51	a	1.20	a
2	0.42	a	0.34	ab	165.44	a	4320.85	a	2705.87	a	487.33	a	10.65	a	1.42	a	0.50	a	0.64	a	0.52	a	0.54	a	0.52	a	1.08	a
3	0.39	a	0.22	b	93.86	a	5409.81	a	2298.71	a	-477.34	a	163.61	a	1.21	a	0.56	a	0.48	a	0.43	a	0.57	a	0.50	a	0.77	a
4	0.48	a	0.39	a	144.87	a	4948.66	a	1895.97	a	938.22	a	-46.15	a	1.23	a	0.52	a	0.59	a	0.58	a	0.54	a	0.54	a	1.09	a
12	0.43	a	0.36	a	109.16	a	4270.77	a	2934.49	a	416.14	a	96.17	a	1.24	a	0.50	a	0.63	a	0.53	a	0.59	a	0.53	a	1.06	a
13	0.40	a	0.30	ab	152.40	a	4708.92	a	3306.03	a	-295.47	a	141.36	a	1.26	a	0.48	a	0.57	a	0.44	a	0.57	a	0.50	a	0.93	a
14	0.44	a	0.40	a	125.00	a	3952.27	a	4091.26	a	-184.82	a	-127.12	a	1.20	a	0.47	a	0.82	a	0.43	a	0.53	a	0.53	a	0.92	a
23	0.42	a	0.32	ab	170.87	a	4625.71	a	2153.32	a	705.23	a	19.38	a	1.32	a	0.51	a	0.54	a	0.54	a	0.50	a	0.52	a	1.09	a
24	0.45	a	0.41	a	154.68	a	4091.64	a	4139.51	a	110.01	a	1.92	a	1.23	a	0.43	a	1.20	a	0.47	a	0.52	a	0.50	a	1.10	a
34	0.43	a	0.35	ab	123.68	a	4371.03	a	3135.50	a	50.85	a	-12.93	a	1.32	a	0.50	a	0.77	a	0.48	a	0.53	a	0.52	a	0.94	a
123	0.42	a	0.32	ab	240.27	a	4347.03	a	2795.78	a	-247.62	a	117.26	a	1.42	a	0.50	a	0.60	a	0.45	a	0.61	a	0.54	a	0.92	a
124	0.44	a	0.39	a	183.21	a	4166.56	a	3257.24	a	530.61	a	92.74	a	1.38	a	0.46	a	0.67	a	0.53	a	0.57	a	0.51	a	1.18	a
134	0.40	a	0.35	a	70.46	a	3654.07	a	3574.26	a	-380.36	a	296.71	a	1.17	a	0.49	a	0.72	a	0.43	a	0.97	a	0.55	a	0.89	a
234	0.44	a	0.34	ab	177.31	a	4658.79	a	2493.28	a	52.48	a	21.05	a	1.21	a	0.54	a	0.60	a	0.50	a	0.56	a	0.53	a	0.98	a
1234	0.44	a	0.33	ab	113.09	a	4652.34	a	2953.96	a	-369.86	a	230.72	a	1.08	a	0.53	a	0.59	a	0.43	a	1.18	a	0.53	a	0.79	a
Mean	0.43		0.35		145.41		4397.42		3008.88		137.72		68.97		1.27		0.50		0.67		0.49		0.62		0.52		0.997	
P value	0.433		**0.000**		0.527		0.619		0.632		0.596		0.776		0.964		0.520		0.52		0.750		0.564		0.892		0.374	

Treatments are monocultures and mixtures of the four early to middle ripening wheat cultivars in an RCBD experimental design with six replicates. Each digit stands for a single cultivar, so the treatment 1234 shows the 4-component mixtures of cultivars 1,2,3 and 4. For definitions of indices, please see the Extended Data Fig. 3, and also the Methods section. Values of each column with similar letters are not significantly different; Tukey, $P<0.05$.

Table S5. Curve characteristics (primary slope indices) of 255–tuple GSM. For more information, please see Figure S3 and Materials and Method section.

Treatments	Total R Slope		Total B Slope		R max slope		B max slope		R_{G} slope		R_{B} slope		R_{G} slope		R_{G} slope		B_{R} slope		B_{G} slope		B_{B} slope		B_{G} slope		B_{B} slope		Total R LSlope		Total B LSlope		R_{G} Lslope		R_{B} Lslope		R_{G} Lslope		R_{B} Lslope		R_{G} Lslope		B_{R} Lslope		B_{G} Lslope		B_{B} Lslope		B_{G} Lslope		B_{B} Lslope	
1	0.894	ab	0.772	ab	2.903	a	4.164	a	0.831	a	0.689	a	0.988	a	1.553	a	2.839	a	0.232	a	0.469	a	1.004	a	2.144	ab	2.060	a	0.888	ab	0.801	a	0.841	a	0.682	a	0.970	a	1.480	a	1.934	a	0.866	a	0.463	a	0.985	a	2.051	ab	1.538	a
2	0.899	ab	0.803	ab	2.697	a	3.848	a	0.908	a	0.688	a	0.981	a	1.550	a	2.255	ab	0.558	a	0.469	a	0.972	a	1.990	ab	2.024	a	0.897	ab	0.823	a	0.999	a	0.681	a	0.964	a	1.480	a	1.740	a	0.991	a	0.462	a	0.954	a	1.914	ab	1.744	a
3	0.905	a	0.809	a	2.231	a	2.998	a	0.831	a	0.720	a	0.975	a	1.435	a	1.709	b	0.484	a	0.436	a	0.962	a	1.738	b	1.370	a	0.900	a	0.826	a	0.820	a	0.713	a	0.958	a	1.375	a	1.407	a	0.851	a	0.428	a	0.947	a	1.684	b	1.188	a
4	0.887	b	0.780	ab	2.930	a	4.314	a	0.863	a	0.683	a	0.961	a	1.620	a	2.345	ab	0.449	a	0.460	a	0.911	a	2.291	a	1.882	a	0.883	b	0.809	a	0.864	a	0.676	a	0.938	a	1.543	a	1.820	a	0.924	a	0.455	a	0.887	a	2.184	a	1.728	a
12	0.893	ab	0.784	ab	3.151	a	4.492	a	0.871	a	0.683	a	0.992	a	1.626	a	2.696	ab	0.509	a	0.459	a	0.967	a	2.145	ab	1.740	a	0.890	ab	0.806	a	0.900	a	0.676	a	0.973	a	1.546	a	1.841	a	0.925	a	0.453	a	0.945	a	2.052	ab	1.257	a
13	0.901	ab	0.791	ab	2.340	a	3.180	a	0.797	a	0.709	a	0.988	a	1.528	a	2.384	ab	0.359	a	0.465	a	0.982	a	1.944	ab	1.780	a	0.895	ab	0.809	a	0.805	a	0.702	a	0.972	a	1.457	a	1.765	a	0.569	a	0.457	a	0.965	a	1.873	ab	1.353	a
14	0.891	ab	0.785	ab	3.147	a	4.449	a	0.867	a	0.680	a	0.994	a	1.611	a	2.587	ab	0.610	a	0.463	a	0.929	a	2.023	ab	1.761	a	0.892	ab	0.810	a	0.953	a	0.673	a	0.974	a	1.524	a	1.872	a	1.103	a	0.457	a	0.902	a	1.930	ab	1.574	a
23	0.901	ab	0.797	ab	2.949	a	4.030	a	0.826	a	0.698	a	0.997	a	1.600	a	2.806	a	0.388	a	0.472	a	1.001	a	2.086	ab	2.181	a	0.896	ab	0.820	a	0.820	a	0.691	a	0.980	a	1.519	a	1.483	a	0.688	a	0.465	a	0.983	a	1.987	ab	1.582	a
24	0.895	ab	0.776	ab	2.874	a	4.373	a	0.870	a	0.694	a	0.965	a	1.598	a	2.769	a	0.440	a	0.473	a	0.927	a	2.090	ab	2.082	a	0.889	ab	0.798	a	0.868	a	0.688	a	0.946	a	1.516	a	1.991	a	0.883	a	0.467	a	0.885	a	1.997	ab	1.613	a
34	0.900	ab	0.794	ab	2.564	a	3.562	a	0.832	a	0.704	a	0.988	a	1.570	a	2.027	ab	0.313	a	0.486	a	0.980	a	2.029	ab	1.604	a	0.895	ab	0.821	a	0.821	a	0.697	a	0.970	a	1.496	a	1.560	a	0.633	a	0.479	a	0.959	a	1.954	ab	1.439	a
123	0.900	ab	0.811	a	2.936	a	4.083	a	0.802	a	0.685	a	1.001	a	1.654	a	2.440	ab	0.394	a	0.488	a	0.976	a	2.007	ab	2.144	a	0.896	ab	0.834	a	0.813	a	0.677	a	0.984	a	1.568	a	1.840	a	0.732	a	0.482	a	0.960	a	1.923	ab	1.765	a
124	0.895	ab	0.759	b	3.086	a	4.635	a	0.833	a	0.691	a	0.988	a	1.611	a	2.566	ab	0.031	a	0.468	a	0.971	a	2.290	a	1.895	a	0.892	ab	0.806	a	0.855	a	0.684	a	0.970	a	1.528	a	1.899	a	0.963	a	0.461	a	0.947	a	2.180	a	1.585	a
134	0.898	ab	0.803	a	2.485	a	3.427	a	0.790	a	0.686	a	0.998	a	1.548	a	2.251	ab	0.466	a	0.476	a	0.958	a	1.938	ab	1.930	a	0.898	ab	0.824	a	0.869	a	0.679	a	0.981	a	1.474	a	1.782	a	0.936	a	0.470	a	0.937	a	1.865	ab	1.507	a
234	0.896	ab	0.794	ab	2.922	a	4.121	a	0.868	a	0.687	a	1.000	a	1.581	a	2.128	ab	0.467	a	0.471	a	0.957	a	2.062	ab	1.681	a	0.892	ab	0.820	a	0.862	a	0.680	a	0.980	a	1.499	a	1.657	a	0.849	a	0.465	a	0.937	a	1.959	ab	1.534	a
1234	0.897	ab	0.801	ab	2.580	a	3.776	a	0.778	a	0.691	a	1.002	a	1.566	a	2.376	ab	0.506	a	0.461	a	0.963	a	1.952	ab	1.918	a	0.899	ab	0.826	a	0.902	a	0.684	a	0.982	a	1.485	a	1.842	a	0.967	a	0.454	a	0.947	a	1.884	ab	1.391	a
Mean	0.897		0.791		2.786		3.963		0.838		0.693		0.988		1.577		2.412		0.414		0.468		0.964		2.045		1.870		0.893		0.815		0.866		0.685		0.970		1.499		1.762		0.859		0.461		0.943		1.962		1.520	
P value	**0.015**		**0.004**		0.433		0.336		0.290		0.187		0.115		0.357		**0.015**		0.433		0.395		0.223		0.071		0.717		**0.045**		0.063		0.551		0.208		0.082		0.353		0.223		0.684		0.391		0.067		0.064		0.669	

Treatments are monocultures and mixtures of the four early to middle ripening wheat cultivars in an RCBD experimental design with six replicates. Each digit stands for a single cultivar, so the treatment 1234 shows the 4-component mixtures of cultivars 1,2,3 and 4. For definitions of indices, please see the Extended Data Fig. 3, and also the Methods section. Values of each column with similar letters are not significantly different; Tukey, P<0.05.

Table S6. Curve characteristics (secondary shape indices) of 255-taple GRM. For more information, please see Figure S3 and Materials and Method section.

Treatments	Mean R&B Slope	Total R slope/ R	Total R slope/ R	R_{12}/R_{11} Slope	R_{13}/R_{11} Slope	R_{14}/R_{11} Slope	R_{15}/R_{11} Slope	R_{16}/R_{11} Slope	R_{17}/R_{11} Slope	R_{18}/R_{11} Slope	Total R-R Lslope	Total R/R Lslope	SR_{12}=trend SR_{11}	SR_{13}=trend SR_{11}	R_{12} Lslope/R$_{11}$	R_{13} Lslope/R$_{11}$	(SR$_{12}$+SR$_{13}$)-SR$_{11}$	(SR$_{12}$+SR$_{13}$)-SR$_{11}$	R trendSlope/R trendSlope	R_{10}/R_{11} Lslope	R_{11}/R_{12} Lslope	R_{11}/R_{13} Lslope	R_{10}/R_{12} Lslope	R_{10}/R_{13} Lslope	R_{11} Slope/ R_{12} Lslope	R_{12} Slope/R_{13} Lslope	R_{12} Slope/R_{14} Lslope	R_{12} Slope/R_{15} Lslope	R_{12} Slope/R_{16} Lslope	R_{12} Slope/R_{17} Lslope	R_{12} Slope/R_{18} Lslope	R_{13} Slope/R_{14} Lslope	R_{13} Slope/R_{15} Lslope	R_{13} Slope/R_{16} Lslope	R_{13} Slope/R_{17} Lslope	R_{13} Slope/R_{18} Lslope	R_{14} Slope/R_{15} Slope	R_{14} Slope/R_{16} Slope	Mean total R&B Lslope
1	0.845 a	1.806 a	0.963 a	1.473 ab	0.986 a	0.727 a	0.480 a	0.592 ab	2.255 a	4.574 a	0.087 a	0.902 a	0.013 a	-0.112 ab	1.009 a	0.951 a	0.039 a	-0.034 ab	-3.714 a	1.035 a	0.680 ab	1.015 a	1.386 a	0.796 a	0.988 a	1.010 a	1.018 a	1.049 a	1.470 a	0.347 a	1.012 a	1.020 a	1.045 a	1.387 a	1.116 a	0.756 a	0.845 a
2	0.860 a	1.802 a	0.976 a	1.469 ab	1.010 a	0.781 a	0.481 a	0.579 ab	2.263 a	4.260 a	0.075 a	0.917 a	0.008 a	-0.258 ab	1.005 a	0.882 ba	0.042 a	-0.071 ab	11.862 a	0.862 a	0.679 ab	0.989 a	1.295 a	0.991 a	0.943 a	1.010 a	1.018 a	1.046 a	1.307 ab	0.574 a	1.015 a	1.020 a	1.039 a	1.117 a	1.195 a	0.933 a	0.860 a
3	0.863 a	1.806 a	0.980 a	1.454 a	1.014 a	0.830 a	0.458 a	0.554 b	1.984 a	3.997 a	0.074 a	0.917 a	-0.029 a	-0.454 b	0.980 a	0.720 b	0.023 a	-0.227 b	-18.184 a	1.038 a	0.602 b	0.989 a	1.226 a	0.858 a	1.014 a	1.010 a	1.018 a	1.044 a	1.215 b	0.376 a	1.018 a	1.016 a	1.012 a	1.161 a	1.024 a	0.707 a	0.863 a
4	0.846 a	1.805 a	0.965 a	1.492 ab	1.059 a	0.712 a	0.496 a	0.624 a	2.372 a	5.017 a	0.074 a	0.916 a	0.062 a	-0.026 a	1.043 a	0.990 a	0.106 a	0.103 a	-0.039 a	1.058 a	0.674 ab	0.945 a	1.414 a	0.941 a	0.999 a	1.011 a	1.025 a	1.049 a	1.288 ab	0.501 a	1.012 a	1.026 a	1.048 a	1.083 a	1.180 a	0.789 a	0.846 a
12	0.848 a	1.803 a	0.973 a	1.492 ab	1.029 a	0.764 a	0.492 a	0.600 ab	2.385 a	4.687 a	0.084 a	0.905 a	0.065 a	-0.165 ab	1.044 a	0.920 ba	0.071 a	-0.015 ab	1.612 a	1.017 a	0.671 ab	0.971 a	1.332 a	0.681 a	0.970 a	1.010 a	1.019 a	1.052 a	1.668 a	0.551 a	1.014 a	1.023 a	1.046 a	1.393 a	1.202 a	0.619 a	0.848 a
13	0.852 a	1.807 a	0.978 a	1.530 ab	1.010 a	0.796 a	0.473 a	0.571 ab	2.162 a	4.182 a	0.086 a	0.904 a	0.030 a	-0.321 ab	1.021 a	0.858 ba	0.049 a	-0.106 ab	-4.548 a	0.707 a	0.653 ab	0.992 a	1.280 a	0.766 a	0.991 a	1.010 a	1.017 a	1.049 a	1.351 ab	0.635 a	1.017 a	1.018 a	1.037 a	1.338 a	1.220 a	0.745 a	0.852 a
14	0.851 a	0.999 a	0.970 a	1.471 ab	1.071 a	0.800 a	0.490 a	0.598 ab	2.383 a	4.370 a	0.083 a	0.907 a	0.035 a	-0.258 ab	1.022 a	0.884 ba	0.048 a	-0.018 ab	-2.361 a	1.144 a	0.682 ab	0.936 a	1.265 a	0.855 a	0.916 a	1.009 a	1.020 a	1.058 a	1.375 ab	0.546 a	1.012 a	1.031 a	1.049 a	1.147 a	1.248 a	0.840 a	0.851 a
23	0.858 a	1.806 a	0.972 a	1.486 ab	0.998 a	0.770 a	0.484 a	0.585 ab	2.296 a	4.445 a	0.076 a	0.915 a	0.069 a	-0.177 ab	1.049 a	0.924 ba	0.069 a	-0.059 ab	1.190 a	0.844 a	0.673 ab	1.003 a	1.311 a	0.869 a	1.008 a	1.011 a	1.017 a	1.052 a	1.310 ab	0.561 a	1.015 a	1.018 a	1.050 a	1.368 a	1.012 a	0.800 a	0.858 a
24	0.844 a	1.807 a	0.972 a	1.470 ab	1.042 a	0.777 a	0.490 a	0.596 ab	2.384 a	4.443 a	0.091 a	0.898 a	0.061 a	-0.152 ab	1.042 a	0.929 ba	0.096 a	0.044 a	27.203 a	1.012 a	0.679 ab	0.936 a	1.315 a	0.811 a	1.005 a	1.009 a	1.020 a	1.054 a	1.386 ab	0.512 a	1.014 a	1.050 a	1.045 a	1.321 a	1.317 a	0.807 a	0.844 a
34	0.858 a	1.806 a	0.967 a	1.456 ab	1.013 a	0.781 a	0.481 a	0.579 ab	2.212 a	4.201 a	0.074 a	0.918 a	0.061 a	-0.144 ab	1.042 a	0.935 ba	0.072 a	-0.024 ab	-1.476 a	0.773 a	0.687 ab	0.988 a	1.305 a	0.959 a	1.015 a	1.010 a	1.018 a	1.050 a	1.311 ab	0.555 a	1.014 a	1.022 a	1.038 a	1.130 a	1.059 a	0.749 a	0.858 a
123	0.865 a	1.805 a	0.972 a	1.489 b	1.027 a	0.826 a	0.493 a	0.576 ab	2.424 a	4.103 a	0.062 a	0.931 a	0.090 a	-0.161 ab	1.060 a	0.931 ba	0.076 a	-0.029 ab	6.167 a	0.900 a	0.712 a	0.975 a	1.228 a	0.942 a	0.988 a	1.012 a	1.017 a	1.053 a	1.337 ab	0.549 a	1.014 a	1.017 a	1.042 a	1.200 a	1.207 a	0.951 a	0.865 a
124	0.849 a	1.803 a	0.941 a	1.479 ab	1.023 a	0.713 a	0.490 a	0.613 ab	2.338 a	4.896 a	0.086 a	0.904 a	0.063 a	0.002 a	1.045 a	1.009 a	0.074 a	0.062 a	-8.684 a	1.125 a	0.675 ab	0.977 a	1.425 a	0.829 a	0.978 a	1.010 a	1.018 a	1.054 a	1.353 ab	0.274 a	1.015 a	1.026 a	1.050 a	1.201 a	1.245 a	0.744 a	0.849 a
134	0.861 a	1.800 a	0.974 a	1.447 ab	1.043 a	0.800 a	0.478 a	0.574 ab	2.262 a	4.086 a	0.073 a	0.918 a	0.080 a	-0.276 ab	1.000 a	0.877 ba	0.019 a	-0.059 ab	2.688 a	1.069 a	0.691 ab	0.955 a	1.269 a	0.838 a	0.916 a	1.010 a	1.018 a	1.050 a	1.274 ab	0.518 a	1.013 a	1.022 a	1.039 a	1.318 a	1.226 a	0.816 a	0.861 a
234	0.856 a	1.805 a	0.960 a	1.463 ab	1.046 a	0.790 a	0.483 a	0.585 ab	2.305 a	4.378 a	0.072 a	0.919 a	0.027 a	-0.196 ab	1.018 a	0.913 ba	0.038 a	-0.023 ab	28.920 a	0.968 a	0.686 ab	0.956 a	1.304 a	0.917 a	1.009 a	1.011 a	1.020 a	1.053 a	1.291 ab	0.585 a	1.013 a	1.021 a	1.049 a	1.086 a	1.117 a	0.816 a	0.856 a
1234	0.862 a	0.998 a	0.970 a	1.501 ab	1.042 a	0.802 a	0.480 a	0.578 ab	2.271 a	4.249 a	0.073 a	0.918 a	0.021 a	-0.322 ab	1.015 a	0.856 ba	0.033 a	-0.092 ab	-3.456 a	1.025 a	0.664 ab	0.965 a	1.269 a	0.777 a	0.901 a	1.010 a	1.021 a	1.055 a	1.293 ab	0.557 a	1.014 a	1.016 a	1.036 a	0.970 a	1.250 a	0.745 a	0.842 a
Mean	0.854	1.804	0.970	1.486	1.028	0.778	0.483	0.586	2.283	4.293	0.078	0.913	0.039	-0.215	1.026	0.906	0.057	-0.027	2.652	0.972	0.674	0.972	1.308	0.855	0.976	1.010	1.019	1.051	1.335	0.521	1.014	1.021	1.043	1.217	1.188	0.787	0.854
P value	**0.023**	0.497	0.258	0.193	0.318	0.195	0.167	**0.012**	0.146	0.137	0.311	0.274	**0.050**	0.054	**0.048**	0.074	0.501	**0.096**	0.439	0.482	0.141	0.191	0.190	0.483	0.087	0.681	0.364	0.163	**0.001**	0.635	0.159	0.131	0.321	0.210	0.744	**0.003**	0.023

Treatments are monocultures and mixtures of the four early to middle ripening wheat cultivars in an RCBD experimental design with six replicates. Each digit stands for a single cultivar, so the treatment 1234 shows the 4-component mixtures of cultivars 1,2,3 and 4. For definitions of indices, please see the Extended Data Fig. 3, and also the Methods section. Values of each column with similar letters are not significantly different; Tukey, P<0.05.

Table S7. Curve characteristics (x-intersect and limits) of 255–tuple GSM. For more information, please see Figure S3 and Materials and Method section.

Treatments	R x-intercept		B x-intercept		B-R x-intercept		R/B x-intercept		$\%R_{01}$ X-length		$\%R_{12}$ X-length		$\%R_{23}$ X-length		$\%R_{34}$ X-length		$\%R_{45}$ X-length		$\%B_{01}$ X-length		$\%B_{12}$ X-length		$\%B_{23}$ X-length		$\%B_{34}$ X-length		$\%B_{45}$ X-length		X_{B2}-X_{R2}		X_{B3}-X_{R3}	
1	0.667	a	5.333	a	4.667	a	0.156	a	8.366	a	55.425	a	23.007	a	10.458	a	1.503	b	3.203	a	61.634	a	19.542	ab	11.176	a	1.634	b	3.399	a	0.850	a
2	0.667	a	5.500	a	4.833	a	0.125	a	7.974	a	54.837	a	22.484	a	10.654	a	2.353	ab	2.484	a	57.974	ab	21.503	ab	12.092	a	2.614	ab	4.248	a	2.614	a
3	0.500	a	6.167	a	5.667	a	0.088	a	6.928	a	53.987	a	23.203	a	11.242	a	3.660	a	2.680	a	48.954	b	26.601	a	15.163	a	3.725	a	7.386	a	3.987	a
4	0.500	a	7.333	a	6.833	a	0.080	a	8.039	a	59.804	a	17.582	a	10.784	a	2.418	ab	2.222	a	61.438	a	18.497	ab	10.980	a	2.810	ab	3.072	a	2.418	a
12	0.833	a	6.167	a	5.333	a	0.138	a	7.059	a	58.039	a	21.569	a	10.458	a	1.569	b	2.222	a	61.111	a	19.542	ab	12.092	a	1.569	b	1.046	a	2.810	a
13	0.500	a	6.333	a	5.833	a	0.103	a	8.693	a	53.987	a	24.771	a	9.346	a	2.288	ab	3.333	a	55.359	ab	23.529	ab	12.549	a	2.288	ab	4.967	a	3.595	a
14	1.000	a	6.000	a	5.000	a	0.190	a	7.190	a	58.170	a	21.765	a	9.608	a	1.961	b	2.092	a	62.876	a	15.817	ab	12.941	a	2.549	ab	2.941	a	3.922	a
23	0.500	a	7.167	a	6.667	a	0.079	a	8.824	a	55.294	a	22.876	a	9.869	a	2.026	b	2.614	a	56.863	ab	24.248	ab	10.327	a	2.222	ab	4.379	a	0.915	a
24	0.333	a	7.167	a	6.833	a	0.054	a	8.170	a	57.190	a	21.242	a	10.131	a	1.895	b	2.222	a	63.595	a	15.033	b	12.941	a	2.157	ab	3.529	a	5.425	a
34	0.500	a	7.333	a	6.833	a	0.082	a	7.843	a	56.275	a	22.092	a	10.000	a	2.549	ab	2.222	a	58.431	ab	20.131	ab	12.484	a	2.876	ab	3.856	a	2.810	a
123	0.500	a	7.333	a	6.833	a	0.064	a	9.608	a	54.314	a	23.529	a	9.346	a	2.222	ab	2.549	a	57.059	ab	22.484	ab	12.157	a	2.222	ab	2.026	a	2.810	a
124	1.000	a	6.667	a	5.667	a	0.131	a	9.281	a	56.078	a	22.026	a	9.412	a	1.961	b	3.203	a	61.634	a	19.085	ab	10.654	a	2.026	ab	3.203	a	2.222	a
134	1.333	a	6.667	a	5.333	a	0.205	a	6.078	a	56.144	a	23.856	a	9.739	a	2.941	ab	2.484	a	59.216	a	19.608	ab	13.072	a	2.680	ab	1.176	a	3.072	a
234	0.500	a	6.833	a	6.333	a	0.065	a	8.954	a	56.078	a	21.242	a	9.935	a	2.614	ab	3.464	a	57.059	ab	21.111	ab	12.288	a	2.876	ab	3.791	a	3.137	a
1234	0.333	a	6.833	a	6.500	a	0.052	a	7.386	a	57.255	a	21.699	a	9.673	a	2.680	ab	2.680	a	57.451	ab	20.523	ab	13.072	a	2.549	ab	2.484	a	3.268	a
Mean	0.644		6.589		5.944		0.107		8.026		56.192		22.196		10.044		2.309		2.645		58.710		20.484		12.266		2.453		3.434		2.924	
P value	0.547		0.815		0.651		0.562		0.315		0.364		0.640		0.989		**0.000**		0.401		**0.000**		0.077		0.523		**0.038**		0.213		0.360	

Treatments are monocultures and mixtures of the four early to middle ripening wheat cultivars in an RCBD experimental design with six replicates. Each digit stands for a single cultivar, so the treatment 1234 shows the 4-component mixtures of cultivars 1,2,3 and 4. For definitions of indices, please see the Extended Data Fig. 3, and also the Methods section. Values of each column with similar letters are not significantly different; Tukey, $P<0.05$.